TAMPEREEN TEKNILLINEN YLIOPISTO
TAMPERE UNIVERSITY OF TECHNOLOGY

Lauri Pirkkanen

STRUCTURAL ANALYSIS OF A NUCLEAR FUEL POOL STEEL LINER

Master of Science thesis

Examiner: professor Reijo Kouhia
Examiners and topic approved on 4th October 2017

ABSTRACT

LAURI PIRKKANEN: Structural analysis of a nuclear fuel pool steel liner
Tampere University of Technology
Master of Science Thesis, 61 pages
October 2018
Master's Degree Programme in Mechanical Engineering
Major: Applied Mechanics and Energy Technology
Examiner: Professor Reijo Kouhia

Keywords: nuclear fuel pool, structural analysis, nonlinear FEA, fatigue

This thesis looks into the structural behavior of a nuclear fuel pool steel liner under normal and abnormal operating conditions. The pool liner is a welded sheet metal assembly which is supported by concrete embedded anchors and stressed by multiple diverse types of loads. The majority of the stresses are generated by the hydrostatic pressure and temperature of cooling water. Other, more insignificant loads, such as the shrinkage and creep of the concrete pool over time, may not be negligible in some cases but in this study, they have not been taken into account.

In the nuclear industry, the consequences of an unreliable component may cause severe production losses due to long repair times, so many precautions are taken to prevent unintentional downtime. This necessity of high-level safety standards covers also the pool liner assembly and leads to the requirement that no cooling water leakage is acceptable through the weld seams or any other part for that matter. Hence, one of the objectives of this thesis is to find the most unreliable segments of the liner assembly and analyze its structural integrity. Possible leakages of the pools can be detected and located with leakage control system. Necessary water inventory for the safety related functions of the pools will be preserved with watertight pool liner and concrete structures.

The thesis is divided into three sections: The first part covers the standards and design guidelines which are being followed nowadays, when new nuclear power plants are built. These documents offer good comparison point for the analysis results. In the second part of the thesis, the theory and the background for the analysis is dealt with. This includes the introduction of the calculation model and explanation of the applied boundary conditions. The last part contains the analysis results and the discussion on the outcome relevancy.

The nuclear fuel pool and the steel liner analyzed in this thesis are from Olkiluoto nuclear power plant. There are two nearly identical reactor units, OL1 and OL2, so this study is applicable to both of them. The concrete pools of Olkiluoto plant have already been analyzed but the steel liners were not considered. This thesis continues that work and aims to a reasoned conclusion for the liner's fail probability under different conditions.

TIIVISTELMÄ

LAURI PIRKKANEN: Ydinvoimalaitoksen polttoainealtaan teräsvuorauksen rakenneanalyysi

Tampereen teknillinen yliopisto
Diplomityö, 61 sivua
Lokakuu 2018
Konetekniikan diplomi-insinöörin tutkinto-ohjelma
Pääaine: Sovellettu mekaniikka ja lämpötekniikka
Tarkastaja: professori Reijo Kouhia

Avainsanat: polttoaineallas, rakenneanalyysi, epälineaarinen FEA, väsyminen

Tässä opinnäytetyössä tarkastellaan ydinvoimalaitoksen polttoainealtaan teräsvuorauksen rakenteellista käyttäytymistä normaaleissa ja epänormaaleissa käyttöolosuhteissa. Teräsvuoraus koostuu useammasta levystä, jotka on kiinnitetty betonialtaaseen valetuilla juurituilla. Vuorauslevyihin kohdistuu monentyyppisiä rasituksia, joista tärkeimmät ovat vedenpaine ja lämpötilakuorma. Joissain tapauksissa vähäisemmät kuormat kuten betonin kutistuma saattavat vaikuttaa merkittävästi lopputulokseen, mutta tässä työssä ne on perustellusti jätetty pois.

Ydinvoimateollisuudessa viallisten tai epävarmojen komponenttien aiheuttamat seuraukset voivat olla erittäin vakavia, joten suunnitteluun ja käytännön työhön on kehitetty paljon erinäisiä ennaltaehkäiseviä toimenpiteitä. Nämä toimenpiteet koskevat tietysti myös polttoainealtaan vuorauslevyjä. Vuorauslevyjen ja niiden saumojen tulee olla täysin vedenpitäviä sekä normaaleissa, että epänormaaleissa käyttöolosuhteissa. Yksi tämän työn tavoitteista onkin löytää vuorauslevykokonaisuuden heikoin kohta ja analysoida sen kuormankantokykyä.

Lopputyö on jaettu kolmeen osaan: ensimmäisessä osassa käydään pintapuolisesti läpi standardit ja suositukset, joita nykypäivän ydinvoimalasuunnittelussa käytetään. Ne antavat hyvän vertailukohdan lopullisen analyysin tuloksille. Toisessa osassa lopputyötä aihetta avataan tarkemmin ja työssä käytetty teoria esitetään. Tähän kuuluu myös laskentamallien ja reunaehtojen käsittely. Viimeinen osa sisältää laskennan tulokset ja niistä saadut päätelmät.

Tässä lopputyössä käsitellyt vuorauslevyt ja polttoaineallas ovat Olkiluodon ydinvoimalaitoskeskittymästä, laitoksista OL1 ja OL2. Laitokset OL1 ja OL2 ovat lähes identtisiä, joten työn tulokset pätevät molempiin. Betonisten polttoainealtaiden kestävyys epänormaaleilla lämpötiloilla on aikaisemmin analysoitu, mutta teräksisiä vuorauslevyjä ei ole vielä tarkasteltu. Tämä lopputyö jatkaa kyseistä analyysiä teräsvuorauksen osalta. Tavoitteena on löytää perusteltu näkemys vuorauslevyjen kestävyydelle erilaisissa olosuhteissa.

PREFACE

This thesis was written for Sweco Finland and Teollisuuden Voima (TVO) to overcome yet another obstacle in the field of engineering.

I would like to thank Sweco Finland for giving me resources from a laptop to software licenses to write this thesis. In particular, I would like to thank Hannu Nissinen from Sweco and Timo Kukkola and Jori Välilä from TVO who shared their ideas and insights on the topic during our meetings. Likewise, I am grateful to my examiner Professor Reijo Kouhia for his indispensable comments.

Also, I must give recognition to my fiancé who gave me the energy to write this thesis. More specifically, the energy was provided mainly in the form of potatoes, pork, beef, pasta, chicken, various vegetables and occasional beverages with a mean daily value of 9134 kJ. The total amount of energy used to write this thesis would be able to heat the OL1's spent fuel pool cooling water roughly 0.5°C. That is almost one-third of the temperature increase needed to make the wall liner plate buckle, if the numerical simulation is to be believed.

In Ylöjärvi, Finland, on 2 November 2018

Lauri Pirkkanen

TABLE OF CONTENTS

LIST OF FIGURES

SYMBOL DESCRIPTION

A	Elongation after fracture
a	Side length
b	Fatigue strength exponent, side length
c	Fatigue ductility exponent
D	Flexural rigidity, damage parameter
E	Modulus of elasticity
f_{ck}	Compressive strength
f_{ctm}	Mean tensile strength
f_m	Mean compressive strength
G	Shear modulus
g	Dead weight
h	Thickness
MF	Multiaxiality factor
M_x, M_y	Bending moment
N_x, N_y	Normal line force
$N_{x,cr}$, $N_{y,cr}$	Buckling load
N_{xy}	Shear line force
p	Pressure
R_m	Tensile strength
$R_{p0.2}$	Yield strength (0.2 % proof strength)
$R_{p1.0}$	1 % proof strength
TF	Triaxiality factor
w	Deflection

α	Thermal expansion coefficient
γ_{ij}	Shear strain
ΔT	Temperature difference
ε_a	Von Mises strain
ε_f	Fatigue ductility coefficient
ε_{ii}	Normal strain
ε_p	Plastic strain
ε_u	Uniaxial elongation after fracture
ν	Poisson's ratio
ρ	Density
σ_f	Fatigue strength coefficient
σ_{ii}	Normal stress
τ_{ij}	Shear stress
Φ	Side length ratio

1. INTRODUCTION

Since the 1950s nuclear power plants have been producing electricity to national grids all over the world by utilizing fission reaction. In 2015 11% of the world's electricity production was covered by atomic energy. In Finland that number was close to 33% [1].

Electricity consumption is expected to grow in the future. Especially the introduction of electric vehicles may raise electricity usage in transportation. This leads to a demand of reliable and efficient power production systems. Nuclear power has been concluded to be a good option to mass produce electricity while lowering the mean carbon dioxide emissions of the industry. Another upside of nuclear power production is its operating costs. Even though construction costs are quite high, the overall expenses per energy output unit are not so. Especially if environmental costs are taken into account and compared to fossil fuels.

Typical concerns about nuclear power production relate to the safety issues, since the accidents may be very destructive to people and environment. The controversy over nuclear energy has also been right from time to time. The history has seen many minor accidents and a few serious ones, the last being the Fukushima Daiichi accident in 2011. To prevent those kinds of situations from occurring, a lot of safety measures, routines and standards have been created. One of these measures is the requirement for the spent fuel pools to be watertight. This thesis investigates the possible failure modes which could lead to a pool liner leakage and cause a need for power production stoppage. Even though the failure outcome would not be disastrous in this case, sudden repair procedures would be very expensive, and the overall reliability rate of the plant would suffer. By analyzing the structural behavior of the fuel pool liners, a possible maintenance requirement can be predicted, and necessary actions can be taken before failure.

1.1 Background

Olkiluoto nuclear power plant contains two nearly identical reactor units. The first unit (OL1) has been commercially operational since 1978 and the second one (OL2) since 1980 [2]. Typical to nuclear power plants, both units have similar huge water pools in which spent fuel rods from the reactors are cooled down before long-term waste management. The water pools are made of concrete and their insides are covered with austenitic steel liners.

Even though the radioactive fuel rods are kept in the pool water, the water itself doesn't get contaminated [3]. However, the cooling water may contain various particles which are radioactive, so they are actively filtered out of the water. If the steel liner is to break,

the water leakage, which may contain these particles, is collected and detected using leakage control system in the concrete pool. The concrete segment of the pool is also designed to be watertight to prevent the leakage to fully penetrate the pool walls even in a case of liner failure. The impermeability of the concrete part of nuclear fuel pools has been studied for instance in Emil Johansson's Master of Science thesis in 2013 [4]. For Olkiluoto 1 and 2 units, the concrete pool analysis has been done and this thesis is based on the same initial conditions and assumptions as that study [5].

1.2 Objective

Since the design objective of a nuclear fuel storage pool is leak-tightness, sufficient precautions must be taken. Today's national standards can give adequate guidelines for steel liner design engineers, but the given formulae may be too conservative because they have to cover a lot of different situations with a decent safety factor. Additional to that the design standards have been adjusted and developed a lot since the construction of Olkiluoto plants. To find the utilization rate for OL1 and OL2 fuel pool liners, a thorough FEM analysis is done in this thesis.

The main stress components in the liners are induced by hydrostatic pressure of the cooling water and thermal fields acting in the liners. The thermal fields are generated by spent fuel rods which release their thermal energy to the cooling water. Because the liners are fixed to the concrete pool with multiple rigid embedded anchors, they are statically indeterminate and thermal expansion is restricted. This causes stresses in the liner bodies. The liners are relatively thin material so additional to yielding, the liners may fail due to a loss of stability. To find the possible failure modes, nonlinear analysis with small initial perturbations is done.

When the possible failure modes have been found, it is also crucial to discuss their effects in longer time frame since the power plants are still expected to operate for many years into the future. Thus, the possibility of fatigue failure, which may be caused by temperature increases during normal annual fuel replacement procedures and cooling system malfunction, has to be taken into account.

2. STANDARDS AND GUIDELINES

Since power production using nuclear energy sources is not by any means risk-free, it can be made to be a safe and efficient alternative to other sources by controlling the plant production and requiring it to meet various standards. This also covers mandatory maintenance procedures and plant observation. The nuclear industry standards are typically national but they are used interchangeably. This chapter describes briefly some of today's standards.

2.1 YVL

Finnish radiation and nuclear safety authority (STUK) has published Regulatory Guides on nuclear safety and security (YVL) which should be followed when a nuclear power plant is designed and constructed in Finland. These guidelines don't give specific design parameters but rather explain the situations and conditions that must be analyzed in order to show the sufficiency of the structures. For design details, YVL makes references to different national and international standards such as KTA or ASME. [6]

In this study YVL guide is considered and its instructions are followed. The main points regarding fuel pool design are stated in YVL chapter D.3. However as mentioned, YVL gives only a general view of the subject so the steel liners cannot be designed exclusively based on that. For more in detail elements of the analysis, the same standards as YVL leans on, are applied.

2.2 KTA

In Germany, the national standards for nuclear industry is published by The Nuclear Safety Standards Commission (KTA). These standards are similar to Finnish YVL but get more into the design details. Like American ASME standards, KTA standards are commonly used even outside its country of origin.

Fuel pool and steel liner design is covered in chapter 2502. Even though KTA requires only temperature loading to be considered in the liner, this analysis will cover also additional loads. The potential loads for this study are denoted with same nomenclature as in KTA standard and shown in Table 1. According to KTA actions **a** to **g** should be treated as permanent actions (A1), **d**, **e**, **f** and **h** to **l** as variable actions (A2) and **d**, **e**, **h**, **m** and **n** as accidental actions (A3). Some actions are included in multiple groups, so their prevailing group is determined by the magnitude and appearance probability. For instance, temperature action **d** is counted as permanent action when its value is 30°C and accidental when its value is 80°C. [7]

Table 1. *Suggested loading actions for liner design by KTA 2502. Action **j** is missing in the original source as well.*

Nomenclature	Type of Action	Note
a	Dead loads	Self-weight of the assembly
b	Load from weight of water (static pressure of the coolant)	0 – 49 kPa and 118 kPa. See Table 7.
c	Loads from fuel pool internals (e.g. racks, refueling slot gates, inspection equipment	Not applicable to this study.
d	Temperature actions	Stationary 30°C, 45°C and 68°C temperature (KTA standard temperatures: 45°C 65°C and 80°C)
e	Loads from the connecting pipes	Not applicable to this study.
f	Loads from bordering and supported components (e.g., refueling equipment)	Not applicable to this study.
g	Restricted or restrained imposed deformations or movements (e.g. creepage and shrinkage of concrete)	According to TVO's measurements, no concrete drying shrinkage has occurred in Olkiluoto 1&2 fuel pools. Concrete thermal expansion belongs to this category
h	Loads from setdown events (jolts from operational procedures)	Not applicable to this study.
i	Loads from the stored materials (e.g. fuel assemblies, control rods)	Not applicable to this study.

k	Loads from transportation or storage containers (e.g., fuel element casks) including lifting accessories, load-bearing equipment and hoisting gear	Not applicable to this study.
l	Loads caused by movements of the slot gates (e.g., friction forces)	Not applicable to this study.
m	Loads from external events (e.g., design basis earthquake in accordance with safety standard KTA 2201.1) including sloshing water	Not applicable to this study.
n	Loads from plant internal design basis accidents (e.g., jet impingement forces)	Not applicable to this study.

As mentioned, KTA requires only temperature loadings when liner is analyzed. To simulate more detailed behavior of the steel liners, additional loads have to be taken into account. Since the objective in this study is not to design a new structure but to simulate the behavior of the existing one, loads are tried to be defined as accurately as possible to represent their real-life counterparts. Therefore, the partial safety factors for loads are excluded and safety margin is added only to the results. Table 2 consists of the load combinations that have been considered in this analysis and as a reference partial safety factors required by KTA are also shown. The external loads caused by stored materials, transportation containers or fuel pool internals are excluded since they are not supported by the liner plate. They are based on the requirement categories A1 and A2 of KTA standard.

Table 2. *The reference load combinations for pool liner if it was designed using KTA standard.*

Action #	Load combination
1	$1.35a + 1.00b_{49} + 1.35d_{T=30°C}$
2	$1.35a + 1.00b_{49} + 1.50d_{T=45°C}$
3	$1.35a + 1.00b_{118} + 1.35d_{T=30°C}$
4	$1.35a + 1.00b_{118} + 1.50d_{T=45°C}$

The failure criterion in KTA standard is based on Eurocode's limit state design method. The ultimate limit state and serviceability limit state are checked using material data and corresponding safety factors which in this case are 1.1 for the liner and 1.25 for the weld connections [8]. Eurocode 1993-1-5 recommends ultimate limit state criterion for FEM analyses of plated structural elements:

"The ultimate limit state criteria should be used as follows:

1. for structures susceptible to buckling:
   attainment of the maximum load.
2. for regions subjected to tensile stresses:
   attainment of a limiting value of the principal membrane strain.

> **NOTE 1:** The National Annex may specify the limiting of principal strain. A value of 5% is recommended.
>
> **NOTE 2:** Other criteria may be used, e.g. attainment of the yielding criterion or limitation of the yielding zone." [9]

2.3 ASME

ASME is the American Society of Mechanical Engineers. It has published many standards in the field of nuclear power plant design and safety. These standards are widely accepted and used throughout the industry. In particular for this study, a relevant standard is the ASME BPVC Section III Div 2 [10].

The main requirements for liner design are stated in chapter CC-3122: The liner and its welds shall be designed to withstand the effects of imposed loads and accommodate deformation of the concrete containment without jeopardizing leak-tight integrity. Additionally, the liner shall be anchored to the concrete containment.

In chapter CC-3200, the loads for the nuclear power plant containment, including the liner, are specified. The load categories are close to identical to the categories mentioned in KTA standard but grouped a little different. It is noted in ASME that the thermal effects should be based on the most critical transient or steady state condition. This is not a requirement in KTA but is used as an initial assumption in this analysis.

The load combinations and load factors in ASME differ from the ones in KTA. For every design situation of this analysis ASME suggests a partial safety factor of 1.0 for every load. As mentioned in chapter 2.2, the partial safety factors for loads are excluded to simulate real loads, i.e. their values are set to be 1.0, so they are similar to ASME recommendation. The load categories in ASME are separated in only two groups: Service and factored loads, instead of KTA's A1, A2 and A3 groups. The service loads group is corresponding to KTA's group A1 and factored loads group can be interpreted to be a combination of KTA's groups A2 and A3.

Since the liner is a thin structure, its behavior can be based on plate theory. This is pointed out also in ASME chapter CC-3620. The chapter CC-3720 gives the strain limits which are used to verify the integrity and leak-tightness of the liner. The combined membrane and bending strain limits are 0.4 % for the service load group and 1.4 % / 1.0 % for the factored load group. Also, the membrane strains alone are not allowed to exceed 0.2 % with service loads or 0.5 % / 0.3 % with factored loads. The higher strain limit for the factored load group is compressive strain limit and the lower one is tensile strain limit. These limits are only to be used to validate liner plate integrity, so they are not applicable to the weld seams or other components in the pool assembly. Potential strain peaks in the welds are taken into account in this study by using bilinear elastic-plastic material model and multiplying the resulting strain values by triaxiality factor. This nominal strain is then compared to the uniaxial ultimate strain values. The method is introduced in chapter 3.5.

2.4 Standard summary

The standards used in the design process of nuclear power plant liners have differing approaches. All of them are however developed to ease the required engineering work and to guarantee the serviceability and load bearing capacity of the liners. Even though failure criteria and safety factors differ to some extent, their overall effects are kept quite conservative in all standards. The main design parameter differences between the standards are presented in Table 3.

Table 3. *Main design parameter differences of popular standards.*

	KTA	**ASME**
Load groups	A1, A2, A3. (Permanent, variable, accidental)	Service, Factored. (Permanent, variable/accidental)
Partial safety factor for loads	From 1.0 to 1.5 depending on the load type.	1.0 for every load type
Failure criteria for liner	Criterion from Eurocode. For instance, maximum equivalent strain should be under 5 %.	**Service:** 0.2 % membrane, 0.4 % combined strain. **Factored:** 0.5 % / 0.3 % membrane, 1.4 % / 1.0 % combined strain.

3. THEORY

3.1 Steel liner geometry

The nuclear fuel pool steel liners of Olkiluoto 1&2 units are made of multiple 3 mm austenitic stainless-steel sheets. The sheets are laid against the concrete pool and welded together. Common sizes for the sheets are 1250 mm by 6100 mm for the walls and 1500 mm by 3925 mm or 2675 mm for the bottom of the pool. Naturally, these dimensions vary due to corners, details and irregularities in the structure. The welded steel sheet assembly forms a pool which is 11800 mm long, 6600 mm wide and 12265 mm deep.

Behind the weld seams, there is a concrete embedded L-profile where the sheets are also welded to with square groove weld type. This connection is shown in Figure 1. These welds are assumed to be under intense stresses when the loads are applied to the structure, since they are fixed to the concrete embedded L-profiles and bear all the planar loads from the steel sheets. In this context, term “planar loads” indicate the membrane loads that are acting in the direction of undeformed sheet plane. Because extreme stresses are assumed to occur in the weld seams, possible coolant leaks could be suspected to arise there. To observe and control potential leaks, specific leak detection systems have been installed behind the weld seams during construction of the plant. Even though the pool corner geometry is a little different compared to the straight sections, same principles apply and the planar loads will be borne by the welds. The corner detail is shown in Figure 2.

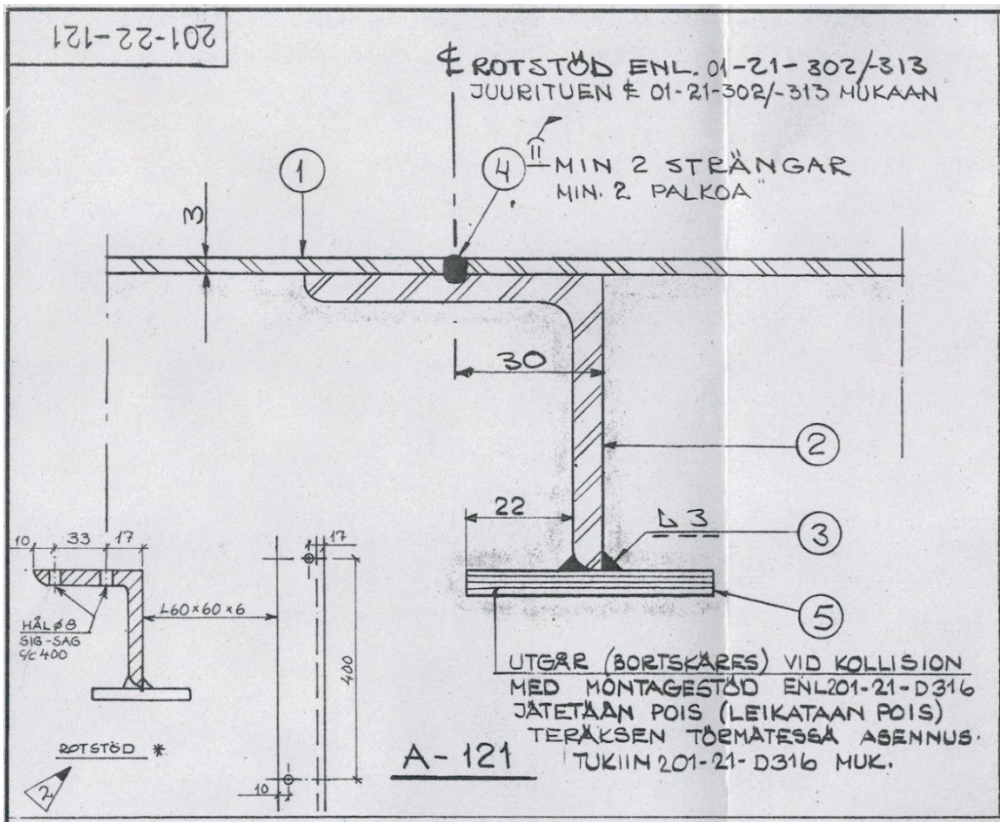

Figure 1. *Weld connection between L-profile stud and liner [11].*

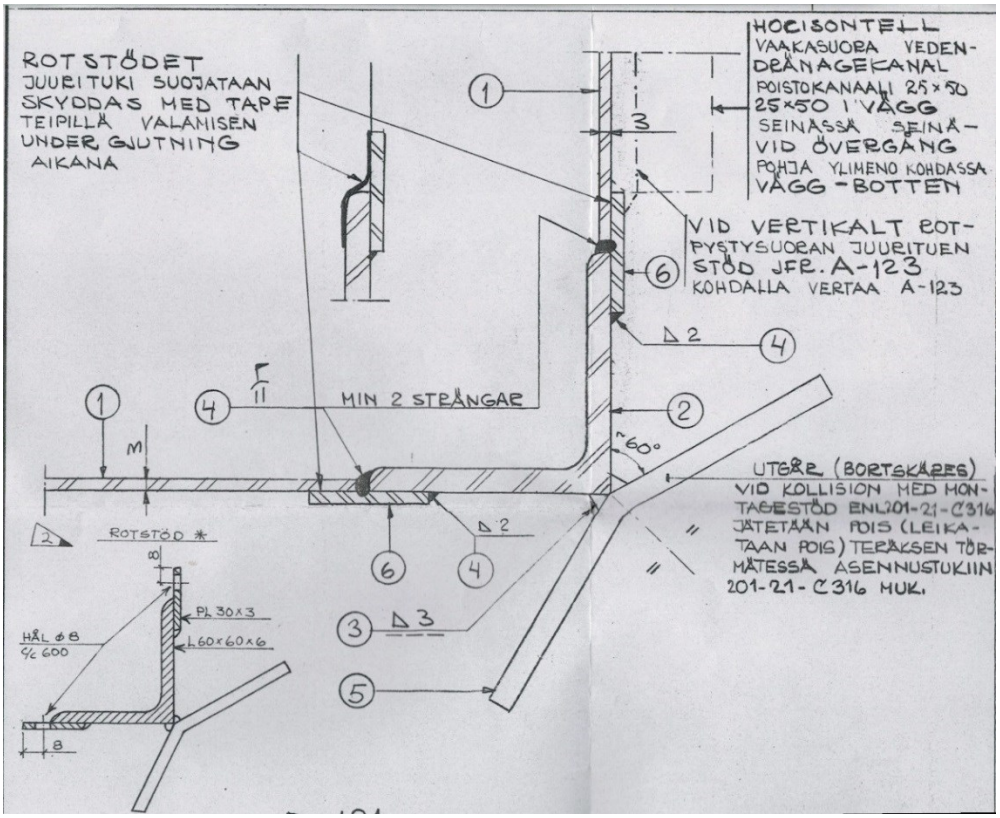

Figure 2. *Weld connection between corner support L-profile and liner plates [11].*

Since the pool liners are made of separate pieces of sheet metal and are connected via concrete embedded L-profiles, it should be a relevant assumption to analyze their structural behavior separately as well. Hence, the main calculation model is limited to a piece of concrete pool, four L-profiles and one 1250 mm wide and 6100 mm long steel sheet with welds. Additional to that, simple supports are applied to weld sides to model the supportive action caused by neighboring liner plates. Even though adjacent liner plates may interact with each other in a way that is not fully covered by using simple supports on weld sides, these boundary conditions should yield conservative results. Simple supports completely restrict the liner expansion resulting in a situation where the stresses get maximized and the buckling load gets minimized. Since the liner plates are very thin compared to their other dimensions it should be a relevant assumption to neglect possible moment interaction between neighboring plates and treat them as membranes. Therefore, simple supports on the sides of the welds are considered to be tolerable boundary conditions.

Two different liner plate positions are simulated: the upmost wall plate position at the cooling water surface and the floor plate position. Either one of these are assumed to be the most critical positions because the plate near water surface is expected to buckle earliest while the plate at the bottom resists buckling most. The top of the pool wall liner is not connected to another liner sheet, so the weld type on that side is fillet weld. This is also modeled into the simulated geometry. Even though in the floor liner assembly all the welds are groove welds, this top fillet weld is used in some simulations to show if weld imperfections have any significant effect on the outcome.

The L-profiles are cast in concrete so their displacements are assumed to follow the concrete pool on their interfaces. As a result, the geometry of the L-profiles can be simplified as plates. Figure 3 shows the analyzed geometry of the calculation model CM1.

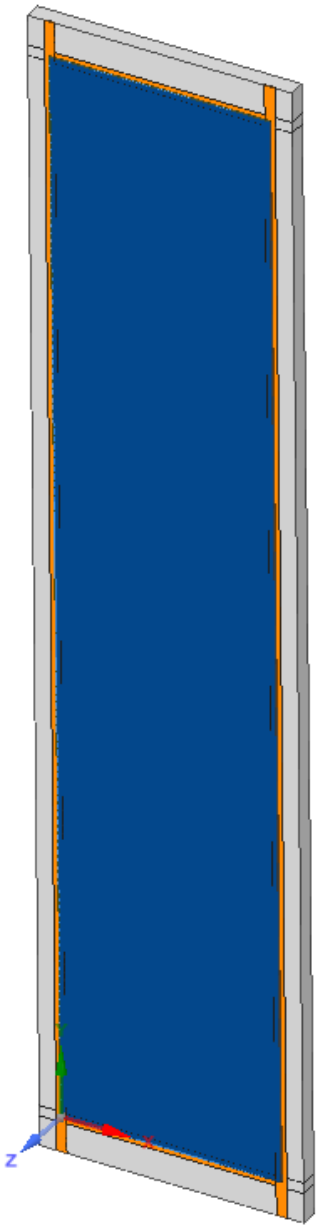

Figure 3. *Trimetric view of the calculation model CM1*

Due to manufacturing tolerances, liner plates are not always against a fully straight concrete slab so the slab may be concave or convex. Convex slab should not yield very distinct result compared to a straight one with initial imperfection since the liner will smoothly grow its displacements away from the slab. However, concave slab may result in a situation where the plate is pushed inwards and the stresses are not to relieved by the large displacement addition caused by buckling. Or at least buckling occurs later than in the situation where the concrete slab is totally straight. To find out if small manufacturing tolerances make any difference, another calculation model (CM2) with 6 mm deep cavity in the concrete slab is created. This allows the liner plate to form a concave shape due to

water pressure before its temperature is started to increase. A section view of the calculation model CM2 is shown in Figure 4. The 6 mm magnitude of the cavity is similar to the initial perturbation magnitude which is discussed and reasoned later in this chapter.

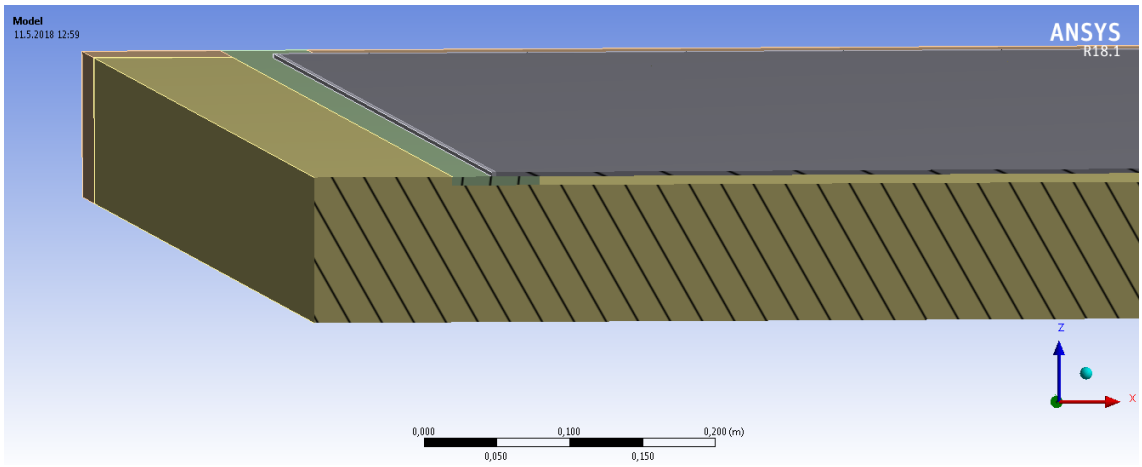

Figure 4. *Section view of the calculation model CM2. Note the 6mm gap between the liner plate and the concrete block.*

Some liner sheets also include anchor plates which support fuel pool internals. These anchor plates are embedded to the concrete pool and welded to the liner. The anchor plates have not been installed consistently in regard to the liner, so they will induce various kinds of buckling shapes. Since the buckling length of the liner decreases with additional supports, buckling can be expected to occur with higher loads than in the main calculation model. The anchor plate liner assemblies are not included in this study.

Material properties for the geometry are presented in Table 4 to

Table 6. The steel structure materials have been gathered from the original assembly drawings [11]. In the drawings, the materials are listed using Swedish standards so they are converted into equivalent Eurocode materials. The original materials for steel liner, L-profiles and welds are SIS 2333-02, SIS 2333 and OK 61.30 respectively. The material properties for stainless steel are gathered from standards SFS-EN 10088-1 [12] and SFS-EN 10088-2 [13] and steel manufacturer Lucefin's technical cards [14]. The fatigue properties are approximated using Bäumel–Seeger uniform material law, which is presented in chapter 3.6. Also, Roessle-Fatemi material model was tested but it led to a slightly more non-conservative result so it was rejected. Weld filler yield strength, tensile strength and elongation after fracture are from weld equipment manufacturer ESAB's welding filler metal handbook [15]. All other weld filler material properties applied, are equal to stainless steel. The concrete pool is cast using K400 grade concrete [5]. The conversion into an equivalent Eurocode strength class has been done in the concrete analysis report, table 5.2. and those properties have been used in this study as well. Even though concrete density is not very important parameter in the analysis, the calculation software requires it. Unreinforced concrete density is set according to concrete analysis report [5].

Table 4. *Material properties of the liner plate and L-profile studs [12], [13], [14].*

1.4301		
Density [1]	$\rho = 7900\ kg/m^3$	T = 20°C
Modulus of elasticity [1]	E = 200 GPa	T = 20°C
	E = 194 GPa	T = 100°C
Yield strength (0.2 % proof strength) [2]	$R_{p0.2} = 230$ MPa	T = 20°C
	$R_{p0.2} = 157$ MPa	T = 100°C
1 % proof strength [2]	$R_{p1.0} = 260$ MPa	T = 20°C
	$R_{p1.0} = 191$ MPa	T = 100°C
Tensile strength [2]	R_m = 540 MPa to 750 MPa	T = 20°C
Elongation after fracture (2)	A = 45 %	T = 20°C
Poisson's ratio (3)	$\nu = 0.24$	T = 20°C
Thermal expansion coefficient (1)	$\alpha = 16*10^{-6}$ 1/K	T = 20°C
Fatigue strength coefficient	σ_f = 810 MPa to 1125 MPa	T = 20°C
Fatigue strength exponent	b = -0.087	T = 20°C
Fatigue ductility coefficient	ε_f = 0.535 to 0.612	T = 20°C
Fatigue ductility exponent	c = -0.58	T = 20°C

Table 5. *Material properties of the weld filler [15].*

OK 61.30		
Density [1]	ρ = 7900 kg/m^3	T = 20°C
Modulus of elasticity (1)	E = 200 GPa	T = 20°C
	E = 194 GPa	T = 100°C
Yield strength (0.2 % proof strength)	$R_{p0.2}$ = 430 MPa	T = 20°C
Tensile strength	R_m = 580 MPa	T = 20°C
Elongation after fracture	A = 45 %	T = 20°C
Poisson's ratio (1)	ν = 0.24	T = 20°C
Thermal expansion coefficient (1)	$\alpha = 16*10^{-6}$ 1/K	T = 20°C
Fatigue strength coefficient	σ_f = 810 MPa to 1125 MPa	T = 20°C
Fatigue strength exponent	b = -0.087	T = 20°C
Fatigue ductility coefficient	ε_f = 0.535 to 0.612	T = 20°C
Fatigue ductility exponent	c = -0.58	T = 20°C

Table 6. *Material properties of the concrete slab [5].*

	K400
Density (1)	$\rho = 2400$ kg/m^3
Mean modulus of elasticity	E = 33 GPa
Compressive strength	f_{ck} = 32 MPa
Mean compressive strength	f_m = 40 MPa
Mean tensile strength	f_{ctm} = 3 MPa
Poisson's ratio (1)	$\nu = 0.2$
Thermal expansion coefficient (1)	$\alpha = 10*10^{-6}$ 1/K

3.2 Loads

The types of loading actions which are applied to the calculation model, are listed in Table 7. From that list, the hydrostatic pressure and temperature actions will yield the largest loads. The nuclear fuel pool is approximately 12 m deep so the pressure generated by coolant water is quite considerable. Even though the pressure is high on the bottom, it is not borne by the steel liner. Since the steel liner is installed against the concrete pool, the hydrostatic force goes through the liner and the concrete part of the pool serves as a support. However, if a liner plate buckles outwards due to a temperature increase, the high water pressure may induce significant stresses in the liner. For different operation temperatures water density varies but the variance is very small so it has been neglected from the analysis.

When used nuclear fuel is moved from the reactor to the fuel pool, it stays subcritical but still generates a good amount of decay heat. To keep the temperatures moderate, coolant water is circulated through fuel racks. In normal operating conditions, coolant water stays at 30°C. However, in this analysis, the coolant is assumed to reach 68°C due to a maintenance shutdown when the reactor is fully emptied into the fuel pool in early outage stage. In the calculation model, the temperature growth is executed in four steps from 15°C to 100°C with 30°C, 45°C and 68°C being the middle steps. The last step of 100°C is solved only for speculation purposes and is not presented in this paper. The initial stage of 15°C is chosen because it is the stress-free temperature where the power plant has been initially

built so potential stresses from different thermal expansion of concrete and steel can be taken into account. As a result of an increase in coolant temperature, steel liner, L-profiles, welds and the concrete pool heat up as well. The liner is typically 3 mm thick thermal conductive steel so its temperature field quickly adopts to the temperature of the coolant. Thus, the temperature field in the steel parts is assumed to be uniform and stationary. Even though this assumption holds for the liner and other metal parts, the thick concrete pool walls will not behave in such a way. The initial temperature of the concrete pool is 15°C and it is risen to 30°C during operation of the nuclear plant. Water temperature increase during the maintenance shutdown is relatively fast so the concrete pool does not heat in same pace. The largest restrictive forces are achieved when the concrete parts are still at 30°C but the metal parts have already reached 100°C, thus concrete pool is kept at 30°C even when the coolant temperature rises to 100°C.

Some minor loads are also considered. These include the self-weight of the system and forced displacements due to thermal expansion of the concrete pool. According to measurements made by TVO, no concrete drying shrinkage has been observed in the fuel pools of Olkiluoto 1&2 units due to high relative humidity in concrete [16]. Thus, shrinkage is not applied into the model. Weld seams always contain some residual stresses which are caused by the cooling of weld filler metal. As the filler cools down, it retracts and tensile stresses develop inside it. In this analysis thermal expansion is the leading load in the liner plate and it counteracts the residual tensile stresses in the weld seams. It is thus assumed that neglecting the residual weld stresses leads to a conservative solution.

Table 7. *Applied loads with side notes.*

Dead weight of the liner	g ≈ 1500 N	Buoyancy taken into account
Water pressure (0 – 6 m from the top of the pool)	p ≈ 0 – 49 kPa	Waterline is 1 m below pool edge. Increase in static water pressure is linear.
Water pressure at the bottom of the pool	p ≈ 118 kPa	
Temperature loads in the liner, welds and L-profiles	ΔT = 15°C, 30°C, 53°C or 85°C	Uniform temperature field
Temperature increase in concrete	ΔT = 15°C	Uniform temperature field

3.3 Failure modes

When hydrostatic pressure or any other force that is normal to the steel liner is applied, the loads pass through the liner and are borne by the concrete pool. In this situation, the liner is in compression and the welds are not stressed by much. It is intuitive that no stability issues arise and the liner stays in the elastic region. It can be noted that compressive normal forces don't induce a failure in the liner on their own if their magnitudes are kept reasonable.

However, when thermal expansion of the liner is introduced, there are forces acting parallel to the liner surface due to the restrictive welds. When temperature is increased, the stresses will increase too, and the welds and the liner material may eventually reach plastic region. Despite the fact that the hydrostatic pressure pushes the steel liner against the concrete pool, the liner may lose its stability and settle to a shape of minimum energy if the temperature is increased enough. This buckling phenomenon should be more likely to happen with larger liner sheets in the upper part of the fuel pool since there is a lot less hydrostatic pressure to keep the steel sheet in place.

The potential buckling shapes of the liner may vary depending on the water pressure magnitude, additional weld plate supports, neighboring liner sheet displacement field, manufacturing tolerances, etc. To find the most likely buckling modes, nonlinear-based eigenvalue analysis is done [17]. The pre-stress state is taken from the first step of the analysis, where the thermal actions have not been assigned yet, but all the other loads are already affecting the structure. Only the thermal load is then used as a loading pattern which induces buckling. A few lowest mode shapes of the eigenvalue buckling analysis are used to create initial perturbations for the nonlinear model which in turn shows if these shapes are potential buckling shapes or if they diminish. Additional to eigen mode shapes, a few different initial perturbations, which are considered to be a result of manufacturing tolerances, are applied. The amplitude for the initial perturbations are based on table C.2. of appendix C of EN 1993-1-5 [9]. In this study, the amplitude becomes 1250 mm / 200 ≈ 6 mm.

The initial perturbations are numbered from 1 to 5. Figure 5 toFigure 9 show their distinct shapes. As the combinations of different initial conditions would grow large if all of them were considered, the combinations which seemed most critical were analyzed. This selection was done purely intuitively. The chosen combinations are presented in

Table 8.

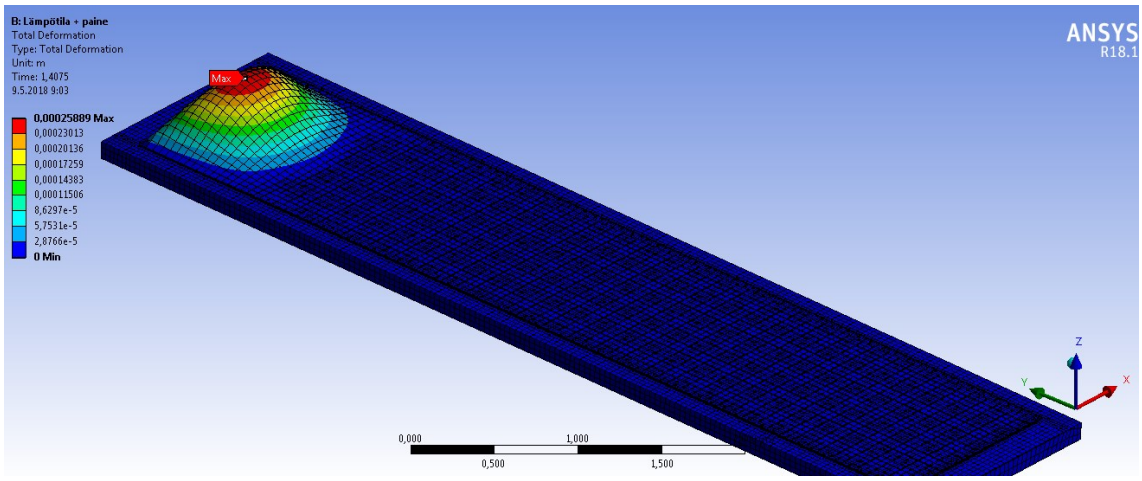

Figure 5. *Initial perturbation 1*

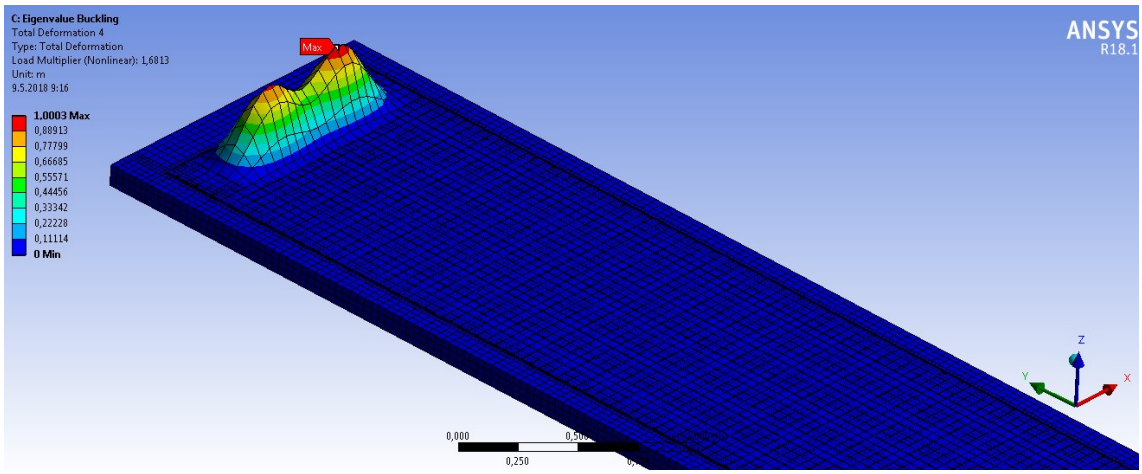

Figure 6. *Initial perturbation 2*

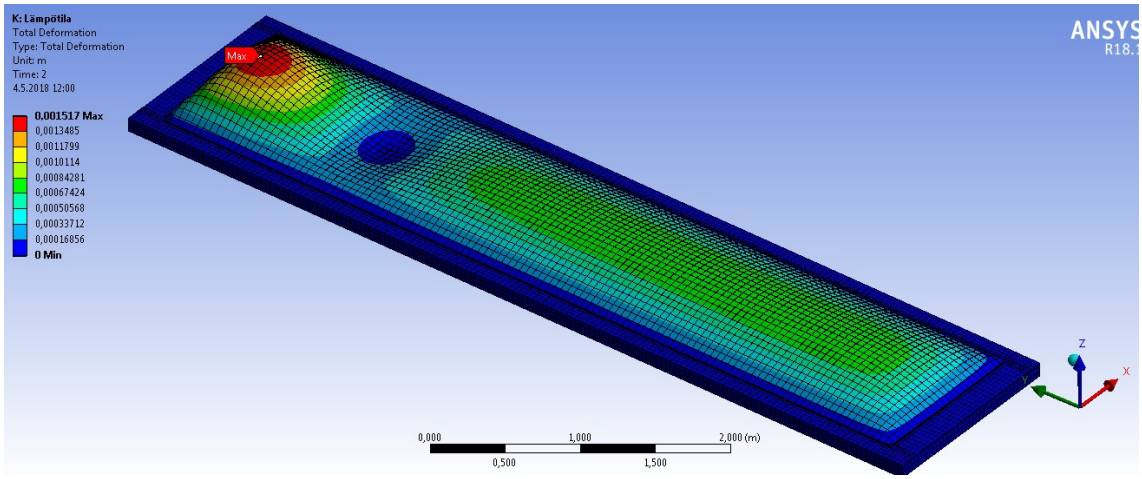

Figure 7. *Initial perturbation 3*

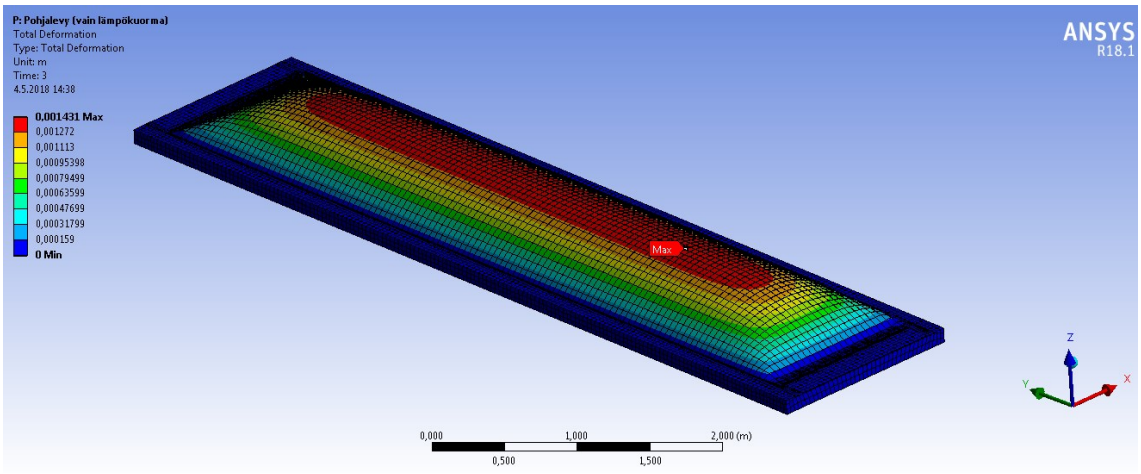

Figure 8. *Initial perturbation 4*

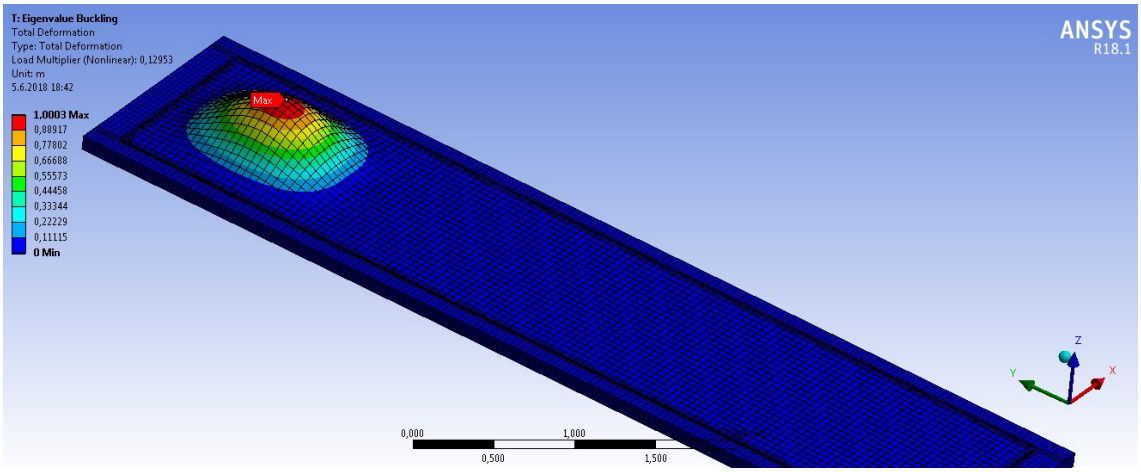

Figure 9. *Initial perturbation 5. This shape is scaled with negative factor to make the perturbation towards the concrete slab.*

Table 8. *Combinations of initial perturbations, calculation models and loading situations that are used. Numbers one and two in the table represent corresponding loading patterns.*

Initial perturbation	CM1	CM2
No perturbation	1, 2	1, 2
1	1	-
2	1	-
3	1, 2	-
4	2	-
5	-	1

The expected behavior of a liner plate under presented loads is summarized under a few main points:

- When total water pressure is applied but thermal load is still small, the deformations are elastic and linear, and no buckling has yet occurred.
- After some temperature increase the plate buckles and this leads to geometrical nonlinearities in the analysis. Buckling is allowed if structural integrity is maintained.
- As the thermal loads keep growing, eventually stresses in the liner reach yield strength and material nonlinearities arise.
- When the plastic deformations are high enough, the liner assembly completely fails.

3.4 Analytical solution

Even though the finite element solvers of today can simulate exceedingly complex structures, it is recommended to verify the results with simpler methods which can be tracked more easily. FEM solvers may yield odd or invalid results due to numerical error, singularities, bad definition of the problem, accuracy error, bugs in software and other issues which are not always user influenced. In this case, the buckling temperature and stress development of the liner plate assembly can be approximated using analytical plate theory and generalized Hooke's law.

3.4.1 Buckling

To find out the buckling temperature of the liner, a linear buckling load is solved. Analytical plate buckling and deflection have been researched a lot and many papers and textbooks cover the subject well. The linear partial differential equation for deflection in a rectangular plate is

$$D\left(\frac{\partial^4 w}{\partial x^4} + 2\frac{\partial^4 w}{\partial x^2 \partial y^2} + \frac{\partial^4 w}{\partial y^4}\right) = p + N_x\frac{\partial^2 w}{\partial x^2} + N_y\frac{\partial^2 w}{\partial y^2} + 2N_{xy}\frac{\partial^2 w}{\partial x \partial y}, \quad (1)$$

where w is the plate deflection in the direction of plate normal, x and y are coordinates along the plate, p is pressure in the direction of plate normal and N_x, N_y and N_{xy} are line forces acting on the plate plane as in Figure 10 [18]. Flexural rigidity D in the governing differential equation (***1***) is a combination of material parameters and plate thickness and is given by

$$D = \frac{Eh^3}{12(1-\nu^2)}. \quad (2)$$

In the flexural rigidity expression E is the elastic modulus, h is the thickness and ν is the Poisson's ratio of the plate.

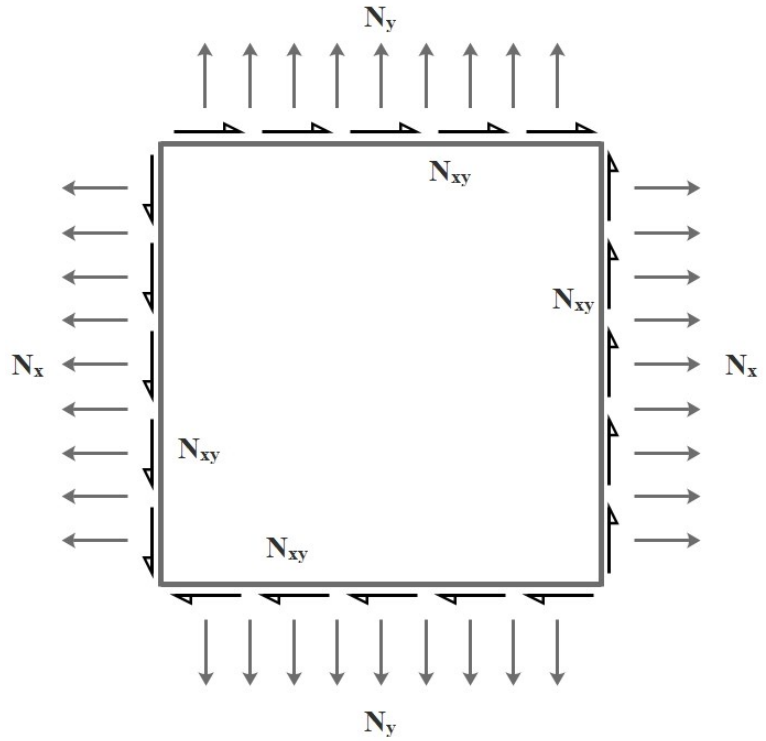

Figure 10. *Normal line forces N_x and N_y, and shear line forces N_{xy}.*

For the sake of simplicity, uniformity of the line loads caused by temperature change is assumed. Additional to that, the loads are assumed to be only compressive i.e. potential

shear forces are neglected and directional expansion is assumed to be borne only by the corresponding ends. These assumptions should not be very much off the reality since the welds and the L-profiles expand roughly the same amount as the liner.

Even though the liner plate is welded to the L-profiles and the rotations are unified, simple support boundary conditions are used for the first analytical model. This yields conservative results because buckling is more likely to happen when the plate's boundary rotations are freed. It also leads to a lot simpler solution compared to clamped boundaries. The boundary conditions for simple supports are

$$w(0,y) = w(a,y) = M_x(0,y) = M_x(a,y) = 0 \tag{3}$$

and

$$w(x,0) = w(x,b) = M_y(x,0) = M_y(x,b) = 0 \tag{4}$$

when a plate with side dimensions of a and b is considered. The moments can be expressed as functions of deflection

$$M_x = -D\left(\frac{\partial^2 w}{\partial x^2} + \nu\frac{\partial^2 w}{\partial y^2}\right) \tag{5}$$

and

$$M_y = -D\left(\frac{\partial^2 w}{\partial y^2} + \nu\frac{\partial^2 w}{\partial x^2}\right). \tag{6}$$

Guess for *w(x,y)* which satisfies the boundary conditions can be found to be

$$w(x,y) = \sum_{m=1}^{\infty}\sum_{n=1}^{\infty} a_{mn}\sin\left(\frac{m\pi x}{a}\right)\sin\left(\frac{n\pi y}{b}\right). \tag{7}$$

When required differentiations are made to the guess and they are substituted into equation (***1***), the result after simplifications is

$$N_{x,cr} = -\frac{\left[\left(\frac{m}{\Phi}\right)^2 + n^2\right]^2}{\left(\frac{m}{\Phi}\right)^2 + rn^2}\frac{\pi^2 D}{b^2}, \tag{8}$$

where Φ is side ratio a/b and r is line force ratio N_y/N_x. Equation (***8***) gives the buckling load for different mode shapes which are determined by parameters m and n. The lowest buckling load can be found by differentiating the equation with respect to m and n, and showing that the function is monotonically decreasing in its domain (due to the minus sign which shows that the force is compressive). Since it is monotone, the minimum

(mathematical maximum) buckling load occurs with minimum *m* and *n* parameters. Both parameters *m* and *n* are defined to be integers with a value of 1 or larger so their minimum value is 1. When these parameters are substituted into equation (*7*), the deflection can be observed to form one half of the sinusoidal cycle to both directions. In other words, the liner's lowest buckling mode is a one-peaked round bubble.

Since the line loads N_x and N_y were assumed to be equal, *r* in equation (***8***) is 1. For simple supported analytical model, the approximate critical buckling load and buckling stress are 3147 N/m and 1.049 MPa respectively when material properties and dimensions are substituted. When the buckling stress is substituted into equation (***15***) and water pressure p_w is assumed to be 0, buckling temperature is obtained. According to this analytical model and stress-temperature relationship introduced in chapter 3.4.2, the increase in the temperature is only 0.25°C after which the plate buckles.

The boundary conditions for clamped plate edges are

$$w(0,y) = w(a,y) = \frac{\partial w(0,y)}{\partial x} = \frac{\partial w(a,y)}{\partial x} = 0 \tag{9}$$

and

$$w(x,0) = w(x,b) = \frac{\partial w(x,0)}{\partial y} = \frac{\partial w(x,b)}{\partial y} = 0. \tag{10}$$

Even though these boundary conditions lead to a much more complex solution when valid guess is substituted into the governing differential equation, it is possible to find the solution using energy balance. Since the elastic strain energy of bending must be in balance with the external work done by the line loads, the buckling load can be evaluated. The derivation is not included in this paper but can be found from the literature [18]. If it is assumed that the shape of the plate does not differ much from a square and that the line loads are close to equal, with sufficient accuracy the deflection can be expected to be represented by equation

$$w = \frac{\delta}{4}\left(1 - \cos\frac{2\pi x}{a}\right)\left(1 - \cos\frac{2\pi y}{b}\right). \tag{11}$$

It should be noted that in this equation, the buckling shape is assumed to be somewhat similar to the shape of the first buckling mode of the simple supported plate i.e. one-peaked bubble, but the boundary conditions for clamped edges still hold. The shape of the equation (***18*** is shown in Figure 11. When energy balance for this deflection guess is written and simplified it results to

$$N_{x,cr} + \frac{a^2}{b^2}N_{y,cr} = \frac{4}{3}\pi^2 D a^2 \left(\frac{3}{a^4} + \frac{3}{b^4} + \frac{2}{a^2 b^2}\right). \tag{12}$$

In this thermal expansion case, the line loads for each side were assumed to be equal so $N_x = N_y$. For clamped edges, the critical buckling load is approximately 11919 N/m and the derived buckling stress is 3.9731 MPa. The yielding buckling temperature increase is then 0.94°C which is almost four times the temperature increase predicted by the simple support model but still very low.

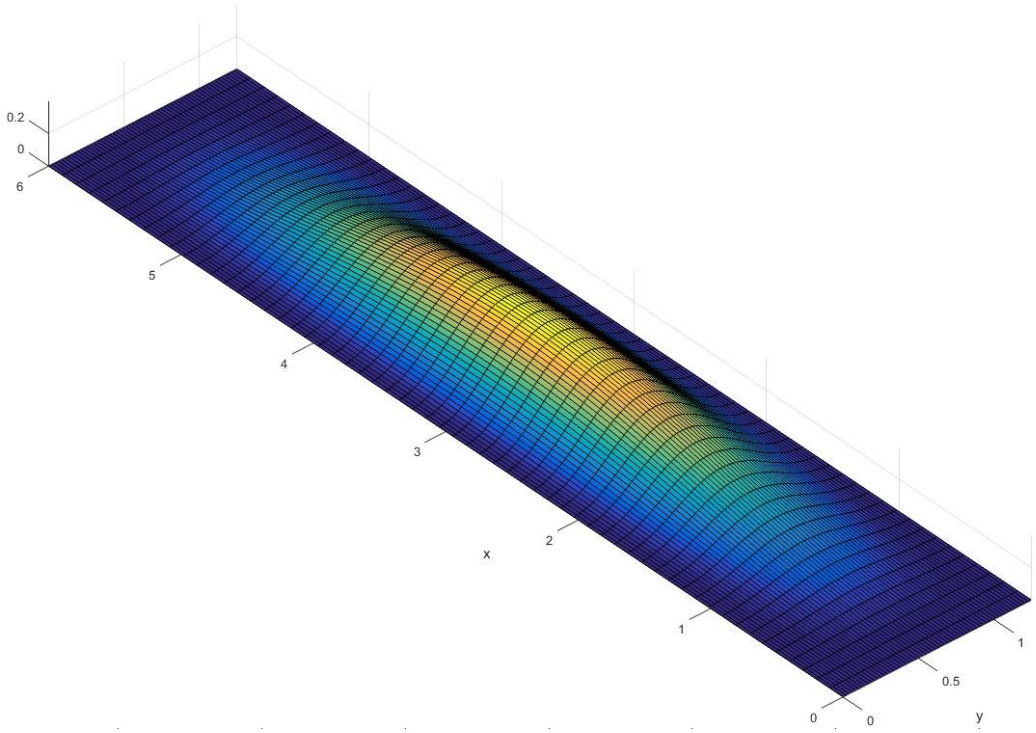

Figure 11. *Buckling shape of a plate with clamped boundaries. The shape is based on equation (*11*).*

Because some simplifications had to be done and water pressure, concrete wall and exact boundary conditions were neglected, the analytical model is supposed to yield only approximate results and only for the plates which are near the surface of the cooling water. On the bottom of the fuel pool the results may vary substantially since the water pressure becomes more dominant component. However, the analytic model gives the order of magnitude and mode shape for low, uniform water pressure which can be used to validate the numeric FEM model.

3.4.2 Stress development in the liner plate

When steel liner plate is heated by hot cooling water and the liner's temperature is assumed to stay uniform and material properties homogenous, it expands proportionally equal amount to every direction. If the expansion is restricted, stresses start to build up in the liner. In terms of mechanics, equal situation to restricted heating is the following event

1. Liner is heated unconstrained and let to expand.
2. Liner is forced to its initial shape and size.

Since Hooke's law binds strains and stresses together, the compressive stresses can be evaluated from temperature difference value by applying the introduced principle. The z-direction i.e. the plate's normal however is not restricted so its strain is not known. But since the water pressure is applied to it, the boundary condition for z-direction is not strain but rather pressure. Generalized Hooke's law in three dimensions is

$$\begin{bmatrix} \varepsilon_{xx} \\ \varepsilon_{yy} \\ \varepsilon_{zz} \\ \gamma_{xy} \\ \gamma_{yz} \\ \gamma_{zx} \end{bmatrix} = \begin{bmatrix} \frac{1}{E} & -\frac{\nu}{E} & -\frac{\nu}{E} & 0 & 0 & 0 \\ -\frac{\nu}{E} & \frac{1}{E} & -\frac{\nu}{E} & 0 & 0 & 0 \\ -\frac{\nu}{E} & -\frac{\nu}{E} & \frac{1}{E} & 0 & 0 & 0 \\ 0 & 0 & 0 & \frac{1}{G} & 0 & 0 \\ 0 & 0 & 0 & 0 & \frac{1}{G} & 0 \\ 0 & 0 & 0 & 0 & 0 & \frac{1}{G} \end{bmatrix} \begin{bmatrix} \sigma_{xx} \\ \sigma_{yy} \\ \sigma_{zz} \\ \tau_{xy} \\ \tau_{yz} \\ \tau_{zx} \end{bmatrix}, \tag{13}$$

where ε_{ii} is normal strain, γ_{ij} is shear strain, G is shear modulus of the material, σ_{ii} is normal stress and τ_{ij} is shear stress. Even though some shear strains and stresses may be found near the welds due to restricting boundary conditions, the analytical model neglects them.

If thermal expansion coefficient and temperature difference are denoted by α and ΔT respectively, one-dimensional normal strain can be found by using equation

$$\varepsilon_{ii} = \alpha \Delta T. \tag{14}$$

Isotropic material parameters are used, hence the one-dimensional strain is equal to every direction *x, y* and *z*. This implies that the normal stresses to the restricted planar directions *x* and *y* are also equal.

When equation (***14***) is substituted into Hooke's law with shear components dropped and water pressure p_w is used instead of σ_{zz}, it yields

$$\begin{bmatrix} \alpha \Delta T \\ \alpha \Delta T \\ \varepsilon_{zz} \end{bmatrix} = \begin{bmatrix} \frac{1}{E} & -\frac{\nu}{E} & -\frac{\nu}{E} \\ -\frac{\nu}{E} & \frac{1}{E} & -\frac{\nu}{E} \\ -\frac{\nu}{E} & -\frac{\nu}{E} & \frac{1}{E} \end{bmatrix} \begin{bmatrix} \sigma_{xx} \\ \sigma_{yy} \\ p_w \end{bmatrix}. \tag{15}$$

In this system of linear equations there are three unknowns and three equations, so it yields one unique solution.

The stainless-steel material properties according to Table 4 and the thermal loads according to Table 7 are applied to equation (***15***), and the normal membrane stresses to x and y directions are evaluated in Table 9. Because they are equal, they both are denoted by σ. These stresses are intuitively also the highest principal stresses of this problem since the shear stresses are assumed to be zero. The water pressure used in this calculation is the pressure acting in the bottom of the pool (118 kPa).

Table 9. *Highest principal stresses acting in the liner plate according to Hooke's law.*

ΔT = 15°C	σ = -63.2 MPa
ΔT = 30°C	σ = -126.4 MPa
ΔT = 53°C	σ = -223.2 MPa

When the extremum principal stresses are compared to the buckling stresses acquired in chapter 3.4.1, it can be observed that the thermal expansion induced principal stresses were much higher than the buckling stresses yielded by either of the analytical buckling models. Thus, buckling is expected to arise in the numeric model before yielding when low water pressure is applied.

3.5 Failure criterion

Even though the displacements grow large in the liner when it buckles, the liner still functions properly if the strains stay reasonable. Since the liner is designed to not carry any load but to be a waterproof barrier, the eventual buckling shape does not have an effect to its serviceability. Therefore, buckling is not an issue if the liner integrity is not lost and the plastic strains stay in safe measures.

Uniaxial strain tests show the elongation for various materials at the point of fracture. As shown in Table 4 and Table 5, the elongation after fracture for 1.4301 stainless steel and OK 61.30 weld filler is 45%. However, this value determines only the elongation when the stress state is one-dimensional. Triaxial stress state has a significant impact on the fracture generation, so uniaxial limit is not directly comparable. To take three-dimensional stress state into account, it is proposed to use triaxiality factor to find the relation between uniaxial test results and actual strains occurring in the analyzed geometry [19]. The triaxiality factor is based on the ratio between the first stress invariant and the second deviatoric stress invariant. This means that increase in hydrostatic pressure component of the stress tensor leads to accelerated fracture. The mathematical formulation of the triaxiality factor is

$$TF = \frac{\varepsilon_u}{\varepsilon_a} = \frac{I_1}{\sqrt{3J_2}} = \frac{\sigma_1 + \sigma_2 + \sigma_3}{\sqrt{\frac{1}{2}[(\sigma_1 - \sigma_2)^2 + (\sigma_2 - \sigma_3)^2 + (\sigma_3 - \sigma_1)^2]}}, \quad (16)$$

where ε_u is uniaxial elongation after fracture and ε_a is actual equivalent strain which includes elastic and plastic components of von Mises strain. By multiplying the equivalent strain by the triaxiality factor, nominal strain ε_n can be compared to the uniaxial strain limit and failure in triaxial stress state can be estimated. In this study, the minimum value of the triaxiality factor is taken to be 1 to find a conservative solution. This implies that supporting effect of the existing stress state is neglected. As a side note, the triaxiality factor is easy to integrate into any FEM-software since principal stresses and von Mises stress are always found from solution selection.

The triaxiality factor can also be applied to fatigue analysis by introducing multiaxiality factor MF [20]. The multiaxiality factor is defined by

$$MF = \frac{1}{2 - TF} \quad \text{for } TF < 1 \quad (17)$$

and

$$MF = TF \quad \text{for } TF \geq 1. \quad (18)$$

In this analysis, conservative minimum value of 1 was chosen for the triaxiality factor so the multiaxiality factor is equal to the triaxiality factor in every stress state.

3.6 Fatigue

Coolant temperature in the fuel pool raises above normal operating temperature multiple times during the design life of Olkiluoto 1&2 reactors due to annual fuel rod replacements and maintenances. This cyclic loading generates fatigue which in turn creates favorable conditions for liner assembly failure. The estimated total amount of these cycles is 80, so the liner assembly integrity can be analyzed based on low-cycle or even on ultra-low-cycle fatigue theory [16]. Half of these cycles has already elapsed, so the power plant is expected to withstand still 40 of them.

Low-cycle fatigue is characterized by plastic deformations and small number of loading cycles. With ductile materials, fatigue cracks grow due to local plastic strains, so instead of using stress-controlled method to determine fatigue life, strain is used as a leading parameter. Since the inspected specimen, or in this case the liner assembly, passes its yield strength during the loading cycles, the stress-strain relation is not anymore linear and stress growth is minor compared to the strains.

A commonly used equation to determine fatigue life with large plastic deformations is the Coffin-Manson relation

$$\frac{\Delta\varepsilon_p}{2} = \varepsilon_f\,(2N_f)^c, \tag{19}$$

where $\frac{\Delta\varepsilon_p}{2}$ is the amplitude of the plastic strain cycle, ε_f is the fatigue ductility coefficient, c is the fatigue ductility exponent and $2N_f$ is the number of load reversals to failure [21], [22]. Fatigue ductility coefficient ε_f and fatigue ductility exponent c are material properties which can be obtained through material testing. The Coffin-Manson relation does not take elastic strains into account thus it is only used when the plastic strains are significantly larger than the elastic strains. Elastic fatigue behavior can be included by substituting Hooke's law into the Basquin relation [23]

$$\frac{\Delta\sigma}{2} = \sigma_f\,(2N_f)^b. \tag{20}$$

The outcome then is

$$\frac{\Delta\varepsilon_E}{2} = \frac{\sigma_f}{E}\,(2N_f)^b, \tag{21}$$

where σ_f is the fatigue strength coefficient and b is the fatigue strength exponent. These are also material properties which are obtained through testing. When elastic and plastic components are added together, the fatigue life determined by total strain can be solved using equation

$$\frac{\Delta\varepsilon}{2} = \frac{\sigma_f}{E}\,(2N_f)^b + \varepsilon_f\,(2N_f)^c. \tag{22}$$

In this paper the material fatigue properties are not acquired from material test data sheets. Instead, the Bäumel-Seeger uniform material law is used to approximate them [24]. The approximation rules are

$$\sigma_f = 1.5R_m, \qquad \varepsilon_f = 0.59\psi, \qquad b = -0.087, \qquad c = -0.58, \tag{23}$$

where

$$\psi = 1 \quad \text{for } \frac{R_m}{E} \leq 0.003 \tag{24}$$

and

$$\psi = 1.375 - 125\left(\frac{R_m}{E}\right) \quad \text{for } \frac{R_m}{E} > 0.003. \tag{25}$$

As the tensile strength value for steel is not precise but varies from 540 MPa to 750 MPa, the fatigue strength coefficient and fatigue ductility coefficient vary too. The constant material properties were substituted into equation (***22***) and tensile strength and strain amplitude were varied while numerical values of fatigue life were followed. The strain amplitude was varied from 0.5 % to 2.5 % using 0.5% increments and for every strain amplitude increment, the tensile strength was varied from 540 MPa to 750 MPa using 10 equal sized steps. It was found that when the strain amplitude was equal or under 1%, the most critical tensile strength value was 540 MPa and for strain amplitudes of 1.5 % and above, the most critical value was 750 MPa. Between the strain amplitude values of 1 % and 1.5 % the tensile strength's effect to fatigue life was at most roughly 5 %, thus it can be neglected and whichever extremum value can be chosen. For the fatigue calculations of this study, the tensile strength value of steel was chosen to be 540 MPa for strain amplitudes under 1.5 % and 750 MPa for strain amplitudes of equal or above 1.5%. Even though the tensile strength of weld filler material is stated to be an exact value of 580 MPa [15], the same values as for steel are used when fatigue calculations are done for the welds. This leads to a conservative result.

Equation (***22***) assumes the strain amplitude to be constant over the whole life-cycle. This however is not true in this analysis. During normal annual maintenance shutdowns, the coolant temperature rises only to maximum value of approximately 42°C according to TVO's measurements [25], and during major reactor maintenance when all the fuel rods are removed, the temperature may rise up to 68°C, which is the highest temperature taken into account in this paper. Large temperature increases may also be a consequence of malfunction in the cooling systems. To include variable strain amplitude in fatigue calculations, simple Palmgren-Miner linear damage rule is utilized [26]. This rule estimates the cumulative damaging effect of the cycles to be

$$D = \sum_{i=1}^{j} \frac{n_i}{N_{fi}}, \tag{26}$$

where j is the total number of different strain amplitudes, n_i is the expected amount of i-th strain amplitude cycles and N_{fi} is the amount of i-th strain amplitude cycles that causes failure alone. When damage parameter D increases to 1, the analyzed component is expected to fail. In principle, all strain amplitudes use a fraction of the structure's fatigue resistance according to their magnitude and occurrence amount. These fractions are then added together and compared to the structure's net fatigue resistance of 1 or 100 %.

It should be noted that strain amplitude in this case is not equivalent to half of the strain maximum value because the normal temperature for the liner plates is 30°C. In this temperature, the liner is already under stresses due to water pressure and thermal expansion,

thus some strains already exist in the normal condition. The strain amplitude can be calculated using the strain difference between abnormal higher temperature state and normal 30°C state.

As large single strain amplitude causes decrease in fatigue resistance, it must be analyzed what temperature is allowed for annual maintenance shutdowns after the peak temperature occurrence. Various peak temperatures from 50°C to 68°C are considered and corresponding normal maintenance temperatures for them is calculated. Additional to that 40°C, 42°C and 45°C constant amplitude loadings for next 40 cycles are analyzed to verify existing temperature limits and to inspect liner plate durability without large strain peaks.

4. CALCULATION MODEL

The calculation software used in the analysis is Ansys Workbench 18.1. Thermal field in the liner is assumed to be uniform, so only static structural analysis is run.

4.1 Initial and boundary conditions

As mentioned earlier, only small part of the concrete pool is included in the model. To restrict rigid body motion and concrete expansion, the boundaries of the concrete block are supported with simple supports meaning that one degree of freedom for every boundary is restricted. These and the weld side supports are the only supports in the model. The displacements in L-profiles, welds and in the liner sheet are restricted using contact elements (see chapter 4.3).

If shrinkage was considered in concrete, one way to simulate it would be to let the concrete block shrink unrestricted by assigning colder temperature field to it. Then this displacement field would be applied to the model in its initial phase. However, the measurements made by TVO show that no drying shrinkage has been detected in concrete, so this aspect is not included in the calculation model [16].

The simulation is done in 4 or 5 steps depending on the final temperature. In the first step, all the loads excluding thermal actions are applied. So, the pool, the L-profiles, the welds and the liner are all at 15°C. This replicates the state where the pool is filled with water but the reactor is not yet started and no spent fuel is moved to the pool. After the initial step, the temperature is raised with consecutive 15°C, 10°C, 28°C and 32°C increments with each added increment representing a step or one second pseudo time in the simulation. This is done until the temperature reaches 68°C or 100°C. The temperature of 68°C is assumed to be the highest possible water temperature during the maintenance shutdown but the temperature is risen up to 100°C to find the structural capacity of the liner in the case where 68°C is not enough. Figure 12 shows how the loading actions are applied during the calculation procedure of the floor plate

.

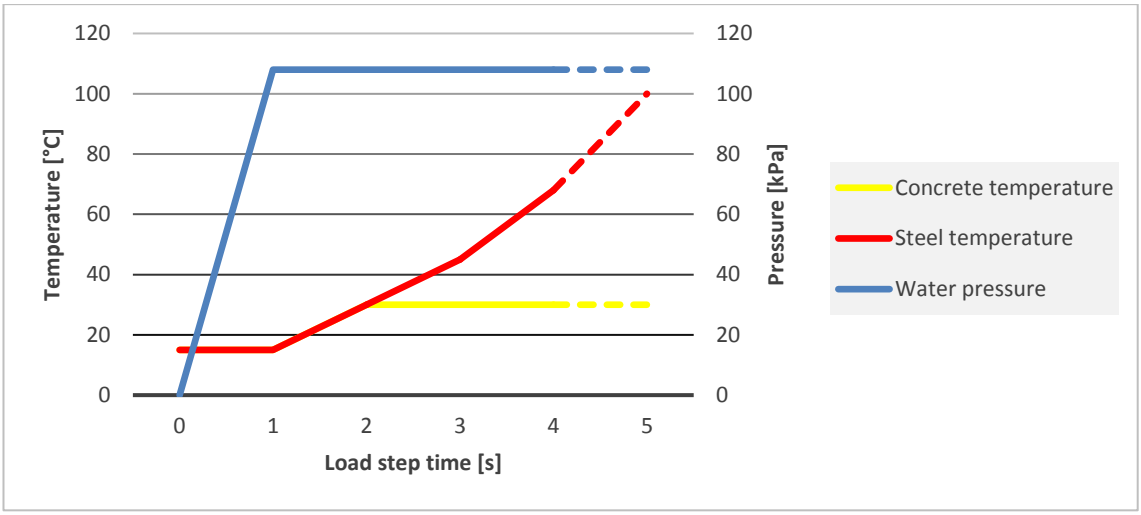

Figure 12. *Loading history during simulation of the floor plates (loading pattern 2). The dashed lines show the loads which were used in speculative calculations only. Their impact is not discussed in this paper.*

4.2 Model simplifications and limitations

Since there were multiple different initial conditions, geometries and loading cases to be considered, extremely fine element mesh was not an option. All the cases were solved with relatively coarse mesh to identify the most critical combinations and to find if the initial perturbations even matter. When the crucial initial conditions and loading cases were found, the element mesh was updated for those geometries.

The effects of the temperature increase on the material properties were mostly neglected since the temperature differences were relatively small. Some validating calculations were done to observe if the variations in the material properties matter. The greatest proportional change due to temperature increase is in the yield strength of stainless steel but some smaller effects can be found in thermal expansion coefficient and modulus of elasticity as well.

The initial imperfections were selected using intuitive approach and eigenmode calculations. This leaves a possibility that the chosen perturbations may not be the most critical ones.

4.3 Element type and model parameters

The geometry is reasonably simple and rectangular shaped, so the meshing is done with hexahedral and quadrilateral elements. The elements in the liner are set to be 8-node solid shells with 3 integration points through thickness to capture plasticity. Solid shell elements capture the behavior of thin and moderately thick structures well and require no extra effort to be connected with other continuum elements. All other parts are meshed with 20-node solid elements. The element mesh is refined in the weld and corner areas

while the middle part of the liner is meshed with relatively coarse mesh. Also, the concrete block is meshed using coarse mesh to keep the calculation time adequate. Since the concrete block exclusively fixes the L-profiles and acts as a one-sided support for the steel liner, its detailed stresses or displacements are not relevant underneath its surface. Additional to that, the behavior of the concrete walls and floor can be expected to be moderate compared to the steel parts. Thus, the coarser mesh inside the concrete shouldn't cause troubles. Sensitivity study for the element mesh was also done. Different mesh densities were tested to verify the results.

As presented in tablesTable 4,Table 5 andTable 6, the materials used in the production of the fuel pool are stainless steel 1.4301 for the metal components, K400 for the concrete block and OK 61.30 is used as a weld filler material. The concrete block is modeled using linear-elastic material model because it is not expected to reach its yield strength before liner failure. After solution the maximum stresses are checked in order to verify this assumption. Elastic-plastic material model is applied for the liner, L-profile studs and the welds. This distributes potential stress peaks and shows the areas where plastic deformations are to be developed. When the plastic material model is not ideal-plastic, it also helps with the convergence issues, which arise from the situations where the yield strength has been attained. For that reason, isotropic linear hardening is included in the material model. The bilinear material model cannot obviously accurately represent true behavior of the materials under different stress conditions since the tangent modulus varies with respect to stress. However, the bilinear model is assumed to be good enough approximation since the plastic regions should not be very widespread or large in magnitude. Tangent modulus is chosen to be 3% of the elastic modulus of the material. This decision is in line with Eurocode suggestions [8], [9].

All model contacts are set to be "bonded" except the liner-concrete and liner-L-profile contacts. In Ansys Workbench bonded contact means that the element nodes in the contact region are kept together i.e. the displacements and rotations between contact faces are equal to every direction and no separation is allowed. In this analysis, the formulation used for linear bonded contacts is multipoint constraint (MPC) instead of the default pure penalty method. In fact, the MPC formulation is not traditional penalty based contact formulation and it does not have contact stiffness since it uses rigid constraint equations. Thus, problems with contact elasticity with higher loads vanish and the contacts may be treated as truly bonded. Liner-concrete and liner-L-profile contacts are modelled as "frictionless" contacts. Frictionless contact lets the liner slide along the concrete block with friction coefficient of zero, thus the liner is not restricted due to friction. This should give conservative results, since the thermal planar loads won't be supported by friction and the loads will be borne by the weld seams. Additional to the friction coefficient being zero, frictionless contact allows the liner to separate from the concrete block making the connection nonlinear. The separation is crucial to stress distribution in the liner and to the

buckling analysis, because the only direction where the displacements can grow unrestricted, is away from the concrete block. Even though the separation is allowed, the liner obviously cannot penetrate the concrete. The frictionless contacts are formulated with augmented Lagrange method to minimize the liner's penetration into other parts but still achieving acceptable calculation times. To enhance convergence, relatively low 0.05 initial normal stiffness factor is chosen and it is set to be updated at every iteration. Due to low normal stiffness factor, penetration between the contact objects has to be checked to ensure valid results. Also, to make the calculation converge better, contact stabilization damping factor is slightly increased and the contact faces are adjusted to touch in the initial stage. Adjust to touch command is however ignored with calculation model CM2 to simulate the cavity's effects. The contact formulations and parameters are shown in Table 10.

Table 10. *Contact types and formulations of the analyzed geometry.*

Contact	Contact type	Formulation	Note
Concrete-L-profile	Bonded	MPC	
L-profile-weld	Bonded	MPC	
Liner-L-profile	Frictionless	Augmented Lagrange	Normal stiffness factor = 0.05
Liner-weld	Bonded	MPC	
Liner-concrete	Frictionless	Augmented Lagrange	Normal stiffness factor = 0.05

The initial calculations are done without large deflection assumption to find out the structural behavior of the model and to get approximate results with shorter calculation time and better convergence. Since the simulation should be as accurate as possible, large deflections are also applied after the initial calculations, thus allowing the nonlinear geometry analysis to show buckling shapes and contact interactions that cannot be generated with small deflection assumption.

If the liner plate buckles, it doesn't necessarily fail because its rigidity is only lost for a small while. To simulate post buckling, nonlinear stabilization has to be added to successfully converge the Newton-Raphson iteration procedure. Arc-length method is not supported for tabular loads in Ansys Workbench, so it cannot be utilized in this analysis instead of nonlinear stabilization [17]. Nonlinear stabilization dissipates element's potential energy in the situations where displacements grow large with smaller load increments, so it works as a sort of damper. If the dissipated energy is large it is obvious that the

calculation results are not correct because the structure is artificially modeled to be too stiff. To verify the result decency, ratio of stabilization energy to element potential energy is tracked. In the post buckling analysis, the energy dissipation ratio, which is used with predicted energies, is set to be a constant value of 1^{-5} to 1^{-2} depending on the stabilization required on different load steps.

5. RESULTS

As the temperature in the analyzed geometry was increased, the displacements began to rise. In the very beginning the displacement growth was, as expected, very slow. The liner plate got compressed due to water pressure and stayed against the concrete slab. When the steel parts were heated enough, in some cases there was a rapid increase in the displacements of the liner plate, thus the plate buckled. In the other cases, the initial perturbation made the displacement growth smoother. The buckling temperature and shape varied a lot depending on the initial conditions. The largest influence was caused by the water pressure. The liner plate on the bottom of the pool buckled with significantly higher temperature compared to the wall plate near the water surface. In these initial results one of the floor plate welds is similar to the wall plate top fillet weld because same calculation model geometry was used for both simulations. This makes the floor plate buckle earlier than with normal groove weld.

The maximum displacement curves for all different initial conditions are presented in figures Figure 13 toFigure 22. It should be noted that the time scale on the x-axis varies from three to five seconds between the simulations. This is due to calculation time limitations and convergence difficulties of some simulations. The convergence difficulties are caused by excessive distortion of the geometry. The last converged time step is shown in the right upper corner of the figures. The integers on the time scale represent the step numbers of the simulation. For instance, “3s” represent the step where the water pressure is applied and the temperature of the steel parts is increased to 45°C while the concrete slab is at 30°C. Since the growth in temperature between the simulation steps is multilinear, the temperature scales in the figures are multilinear as well.

The higher the temperature rose, the higher the stabilization energy had to be to assist the convergence of the iteration procedure. At 45°C the ratio of the stabilization energy to the strain energy of the system was 2.0% at most between the simulations. At 68°C the same ratio was 3.0%. Even though these are considered somewhat acceptable percentages, it should be acknowledged that they generate error to the solution [17]. However, artificial stabilization does not affect the results prior to buckling because it is applied only at the time when the stability is lost. Therefore, stabilization does not interfere with the buckling temperature.

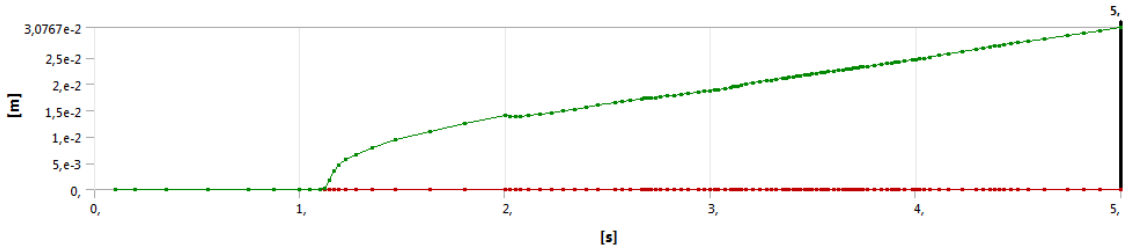

Figure 13. *The maximum displacement curve of the calculation model CM1, loading pattern 1 without initial perturbation. Last converged timestep: 5s. The step from 4 to 5 seconds was only for speculative purposes.*

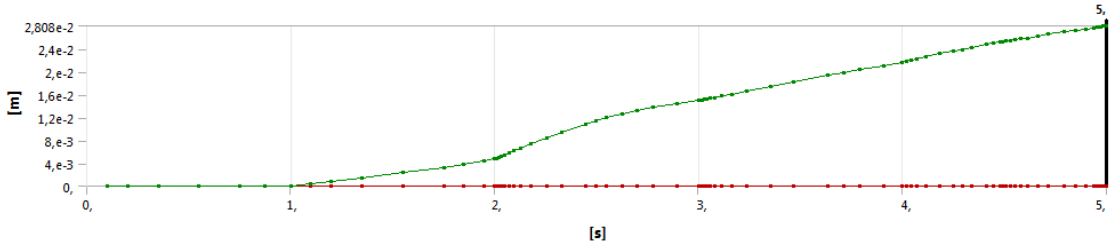

Figure 14. *The maximum displacement curve of the calculation model CM1, loading pattern 1, initial perturbation 1. Last converged timestep: 5s. The step from 4 to 5 seconds was only for speculative purposes.*

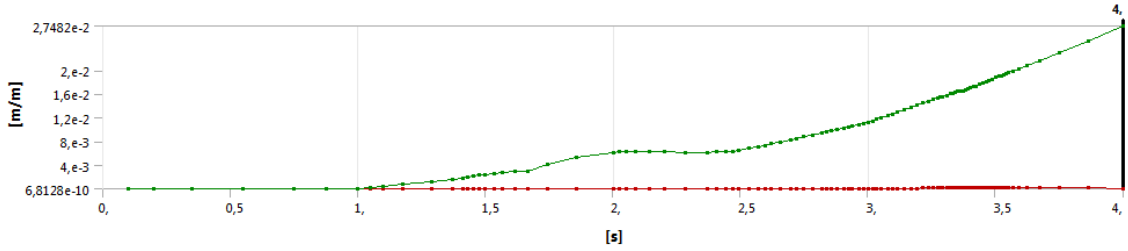

Figure 15. *The maximum displacement curve of the calculation model CM1, loading pattern 1, initial perturbation 2. Last converged timestep: 4s.*

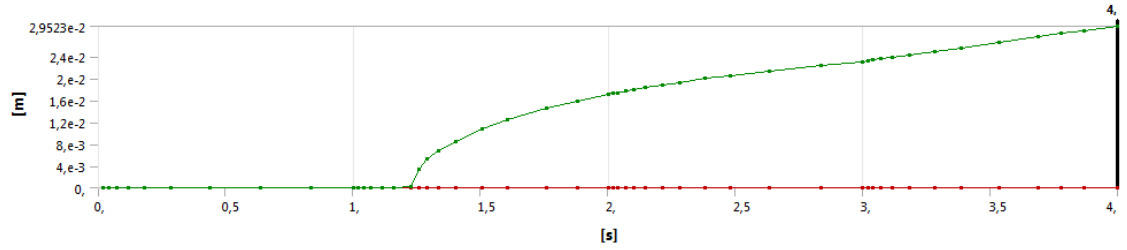

Figure 16. *The maximum displacement curve of the calculation model CM1, loading pattern 1, initial perturbation 3. Last converged timestep: 4s.*

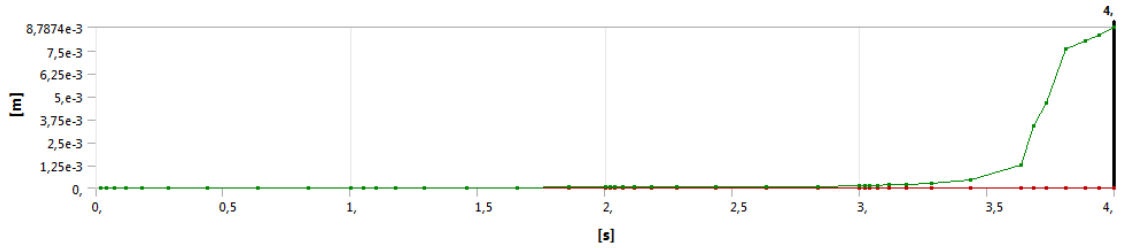

Figure 17. *The maximum displacement curve of the calculation model CM1, loading pattern 2, without initial perturbation. Last converged timestep: 4s.*

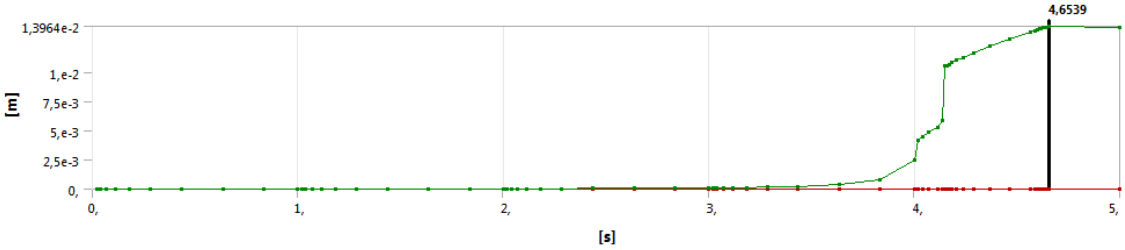

Figure 18. *The maximum displacement curve of the calculation model CM1, loading pattern 2, initial perturbation 3. Last converged timestep: 4.6539s. The step from 4 to 5 seconds was only for speculative purposes.*

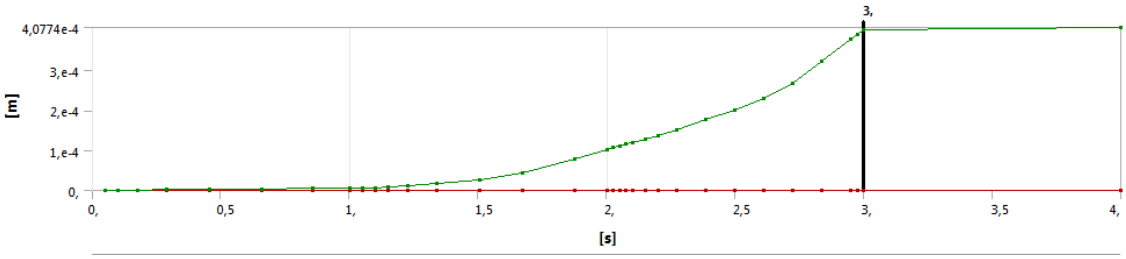

Figure 19. *The maximum displacement curve of the calculation model CM1, loading pattern 2, initial perturbation 4. Last converged timestep: 3s.*

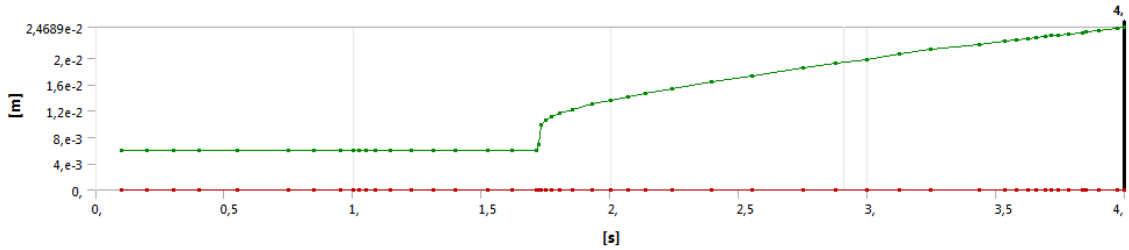

Figure 20. *The maximum displacement curve of the calculation model CM2, loading pattern 1, without initial perturbation. Last converged timestep: 4s. 6 mm initial displacement is due to the 6 mm indentation in the concrete block.*

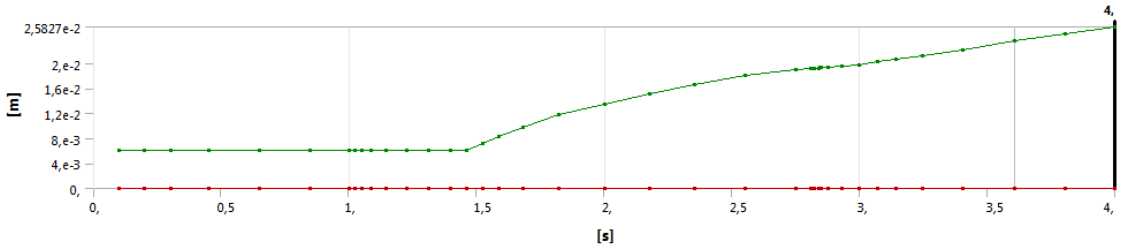

Figure 21. *The maximum displacement curve of the calculation model CM2, loading pattern 1, initial perturbation 5. Last converged timestep: 4s. 6 mm initial displacement is due to the 6 mm indentation in the concrete block.*

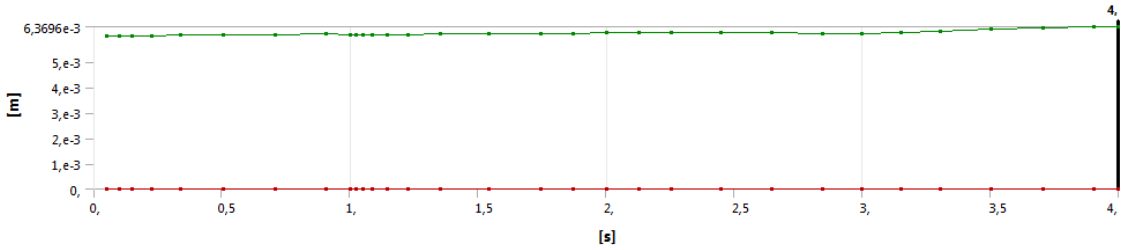

Figure 22. *The maximum displacement curve of the calculation model CM2, loading pattern 2, initial perturbation 5. Last converged timestep: 4s. 6 mm initial displacement is due to the 6 mm indentation in the concrete block.*

The approximate buckling temperatures can be seen from the simulation displacement curves. These temperatures are listed in Table 11. The buckling temperature was not always very clear because the initial perturbation influenced the displacement growth not to have sudden escalations in some cases. Even though the displacement curve didn't show large gradients, for instance in the situation of initial perturbation 1, the deformed shape of the liner plate eventually found its way to similar buckling shape as in the other simulations.

Table 11. *Buckling temperatures of different initial conditions.*

Initial condition (calculation model, loading pattern, initial perturbation)	Approximate buckling temperature
CM1,1, no initial perturbation	16.8°C
CM1,1,1	No sudden displacement growth
CM1,1,2	No sudden displacement growth
CM1,1,3	18.4°C
CM1,2, no initial perturbation	51.5°C
CM1,2,3	51.5°C
CM2,1, no initial perturbation	25.7°C
CM2,1,5	
CM2,2, no initial perturbation	No sudden displacement growth

5.1 Initial results

All the different cases presented in

Table 8 were solved with relatively coarse mesh. The maximum values of resulting total equivalent strains for the whole assembly at the temperature of 45°C, are listed in Table 12, their triaxiality factor corrected counterparts, i.e. the nominal strains, in Table 13 and the maximum equivalent strains of the liner plate in Table 14. The maximum strain for loading pattern 2 is way beyond acceptable and a lot larger than the strains in the other cases. Also, the nominal strain is outside the uniaxial strain limit. This inconsistent result raised suspicions regarding the relevancy of that particular solution. It also failed to converge after 45°C due to large plastic deformations. As expected, the peak strain is found in a geometry discontinuity point where one of the welds end. This is shown in Figure 23. Even though discontinuity points typically create stress and strain peaks, the element mesh can be seen to not be fine enough to capture the strain distribution. To find if the solution is appropriate or not, a finer element mesh was created. Additional to that, the fillet weld was modified to be more realistic. Since the calculation model CM1 was used to model both, liner plate on the pool wall and on the floor, the floor plate top weld was

not accurate. To remove the discontinuity point, the weld was modified as shown in Figure 24.

Table 12. *Total equivalent strain maximums at 45°C of initial coarse meshed model. Results are expressed in percentage form.*

Calculation model CM1	**Loading pattern 1**	**Loading pattern 2**
No initial perturbation	1.37	0.38
1	0.72	-
2	1.12	-
3	0.74	0.39
4	-	27.81
Calculation model CM2		
No initial perturbation	1.34	0.81
5	0.34	-

Table 13. *Triaxial factor corrected equivalent strain maximums at 45°C of initial coarse meshed model. Results are expressed in percentage form.*

Calculation model CM1	**Loading pattern 1**	**Loading pattern 2**
No initial perturbation	3.13	0.38
1	0.97	-
2	1.12	-
3	1.09	0.39
4	-	49.34
Calculation model CM2		
No initial perturbation	1.34	0.81
5	1.10	-

Table 14. *Total equivalent liner plate strain maximums at 45°C of initial coarse meshed model. Results are expressed in percentage form.*

Calculation model CM1	**Loading pattern 1**	**Loading pattern 2**
No initial perturbation	0.14	0.08
1	0.12	-
2	0.16	-
3	0.15	0.08
4	-	0.12
Calculation model CM2		
No initial perturbation	0.15	0.15
5	0.15	-

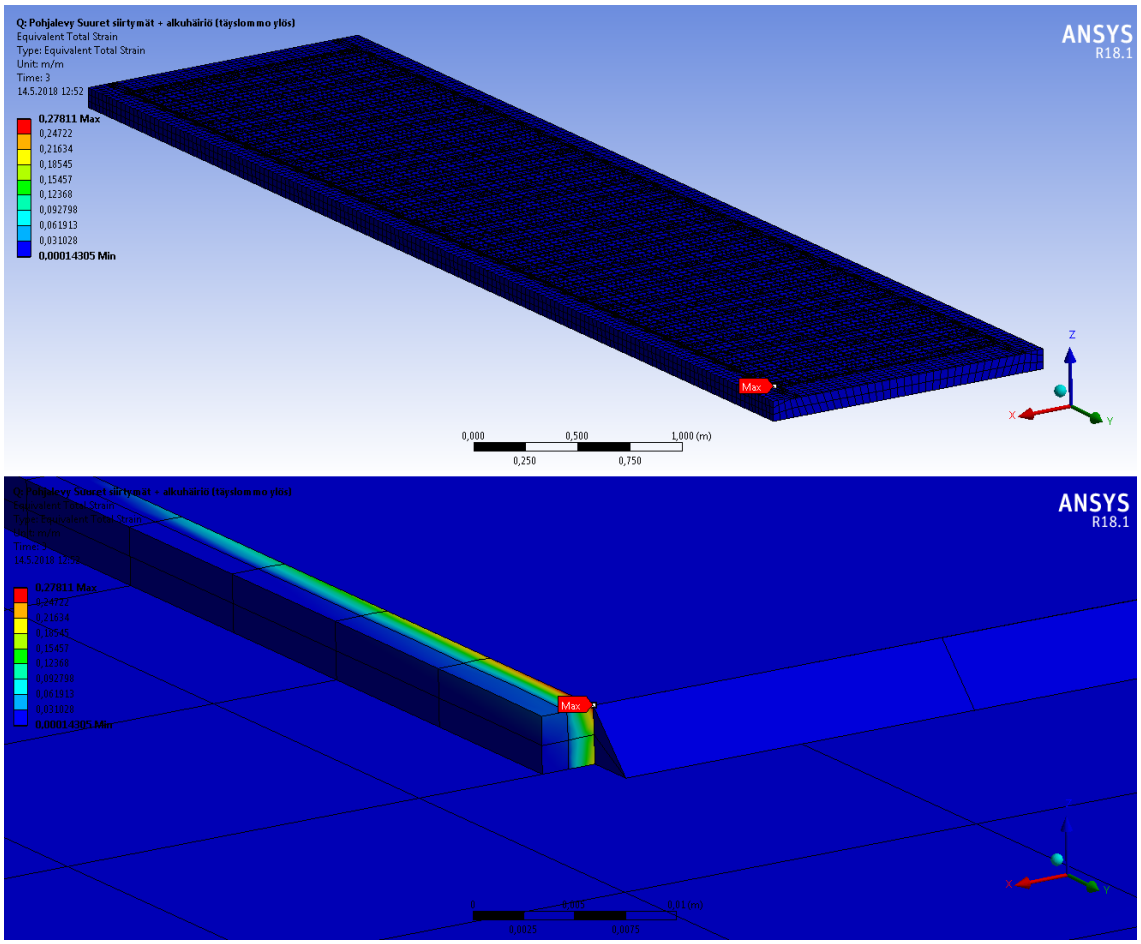

Figure 23. *Maximum equivalent total strain. Calculation model CM1, loading pattern 2, initial perturbation 4. General and close up views.*

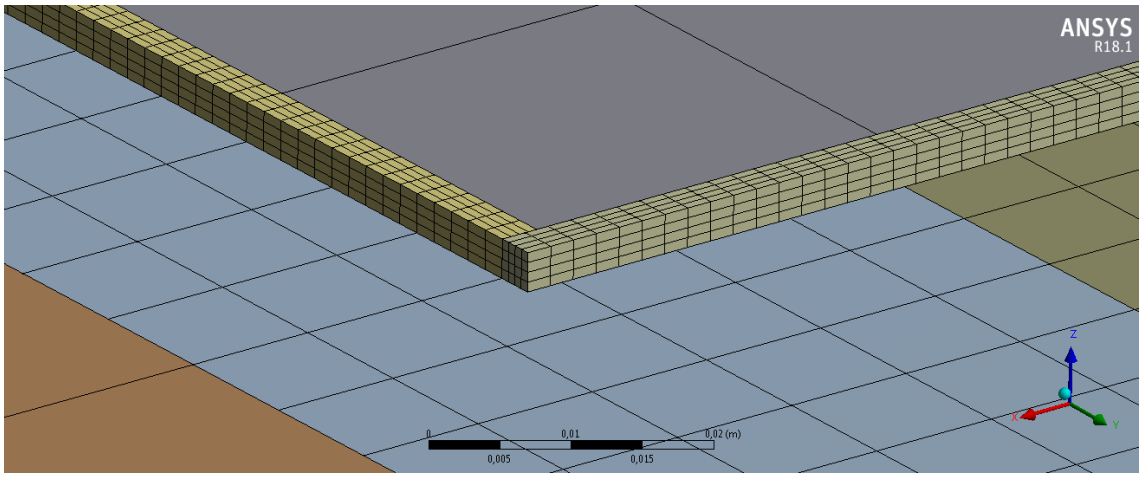

Figure 24. *Mesh refinement and weld modification of calculation model CM1.*

After modifying the weld detail and the element mesh of the model which resulted in a large strain peak, the simulation was run again. The new maximum strain peak seemed more appropriate and consistent with the other initial conditions. The equivalent strain maximum value for the altered model was 0.5656 %.

Since the greatest strain value induced by the loading pattern 2 was shown to be due to a numerical inaccuracy at the discontinuity point, the critical initial condition appears to be the loading pattern 1 without any initial perturbations. To even the strain peak influence, also mean elemental total equivalent strains were checked and they showed similar results. The largest triaxial corrected strain value was found in the side weld near the buckling shape. In that area large deflection gradients in the liner plate cause high bending stresses and eventually also strains in the restricting welds.

It can be noted that the results of the calculation models CM1 and CM2 are quite similar when loading pattern 1 is used, hence the 6 mm deep groove in the concrete slab doesn't make much difference to the final results when the water pressure is low. However, with loading pattern 2, the maximum strain which was found to be in the weld beads, increased significantly when the 6 mm indentation was added. This was due to the concave shape of the liner plate which did not buckle upwards even at 68°C as can be seen in Figure 22. Still the maximum strains were generated with low water pressure due to large deflection gradients in the buckling shape.

As the calculation model CM1, loading pattern 1 and lack of initial perturbation was found to be the most critical combination for the 45°C temperature, the model was remeshed to the same accuracy as in Figure 24 and the simulation was run again. The equivalent strain maximum value at 45°C was 1.2447 % so it was roughly the same as in the coarser model, but the nominal strain grew to 4.9457 %. This was due to a different stress state which was caused by a dissimilar buckling shape compared to the original coarse mesh model. The buckling shape differences are discussed later in chapter 5.3. Even though the buckling shape is not identical to the coarse mesh model, the principal behind the largest nominal strain still is the same. The buckled liner plate bends the side weld and creates favorable regions for failure. The position of maximum triaxial corrected strain value is depicted in Figure 25.

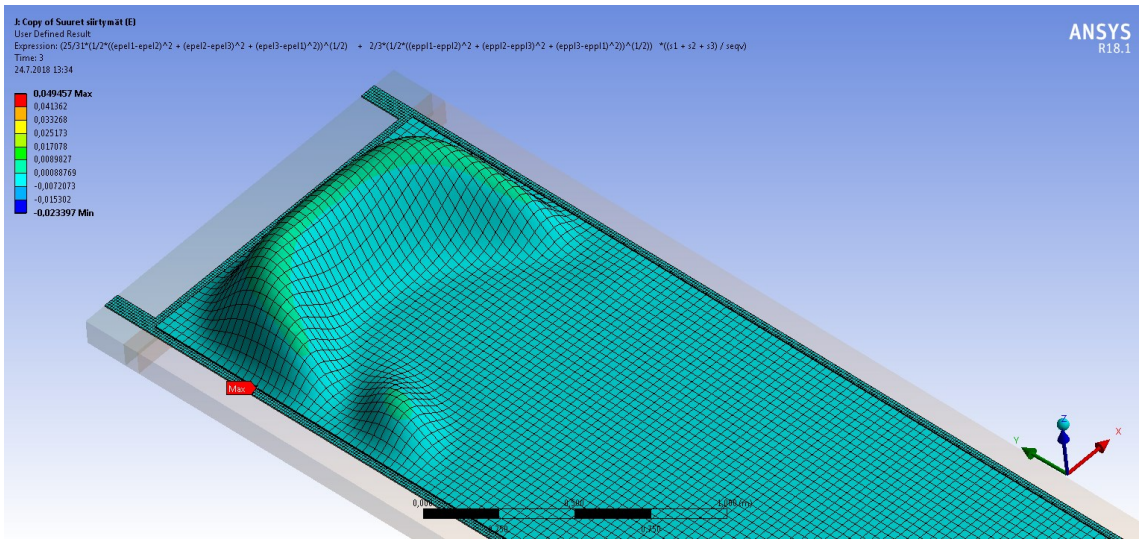

Figure 25. *Maximum triaxial corrected strain value position of remeshed model. The maximum value position is marked with red label. Calculation model CM1, loading pattern 1, no initial perturbation, 45°C.*

5.2 Principal stress development compared to analytical solution

At the temperatures of 30°C, 45°C and 68°C the analytical model predicted both planar principal stresses in the liner plate to be -63.1 MPa, -126.3 MPa and -223.1 MPa respectively. The analytical model assumed the liner plate to stay flat against the concrete slab, so the numerical simulation of the bottom plate should be the most relevant comparison case since the high water pressure holds the plate down. As shown in Table 11, the liner plate stays flat up to 51.5°C.

As assumed for the analytical model, the principal stresses in the FEM results were indeed found to be parallel to the liner plate sides especially in the central region of the plate and for the lower temperatures. The values of the stresses were probed and they seemed also very uniform and similar to the predicted ones. Approximate mean values of the undeformed central regions of the liner plate principal stresses are listed in Table 15. The end of the plate started to buckle at temperature of 51.5°C so the principal stresses of that region are neglected in this comparison because the analytical principal stress calculation doesn't include buckling. It can be noted that the numerical simulation values were almost exactly equal to the analytical predictions meaning that they too increased linearly with respect to the temperature.

Table 15. *Maximum absolute principal stresses in the liner according to the FEM simulation.*

Temperature	Minimum principal stress	Middle principal stress
30°C	-63 MPa	-63 MPa
45°C	-126 MPa	-126 MPa
68°C	-222 MPa	-218 MPa

The positive maximum principal stress values in the bottom liner plate were close to the water pressure as expected. The water pressure on the pool floor is 118 kPa so it is very low compared to the thermal induced stresses, thus plane stress state can be assumed. Von Mises yield criterion for principal plane stress is [27]

$$\sigma_y = \sqrt{{\sigma_1}^2 - \sigma_1\sigma_2 + {\sigma_2}^2}. \tag{27}$$

As noted, the principal stresses are nearly identical to both directions, so von Mises yield criterion can be simplified. The yield criterion is then similar to uniaxial stress state:

$$\sigma_y = \sigma_1. \tag{28}$$

If linear behavior of the principal stresses with respect to temperature is assumed and yield strength of the liner is 230 MPa, yield point is reached at the approximate temperature of 70°C. The elevated temperature however lowers the yield strength of the liner plate and yielding can be assumed to occur at lower temperatures. When linear interpolation between the yield strength of stainless steel at 20°C and 100°C is used, yield point can be solved to be at 61°C. At that temperature the yield strength is approximately 193 MPa. The tangent modulus of steel was assumed to be 3 % of its elastic modulus i.e. 6 GPa, so according to bilinear material model the principal stress increase in the liner after the yield point had been reached would be roughly 95 kPa. The principal strains stay the same even after yielding since they are based on the thermal expansion coefficient as shown in equation (14). In the case of temperature varying yield strength, the analytical model just splits portion of the strain to not be elastic but plastic. The elastic part of the total strain is then 0.732464 % and the plastic part is 0.15536 % at the temperature of 68°C. This cannot be observed in the numerical model since its strains are based on the displacement difference between the initial and deformed geometry.

5.3 Buckling temperature compared to the analytical solution

The analytical buckling calculations predicted almost instant loss of stability when the liner plate's temperature was increased. Even though, the analytical model is not very well comparable to the numerical one since it doesn't include the external support induced by the water pressure, the numerical simulation results showed similar behavior: As can be seen in figures Figure 13 to Figure 16 and in Table 11, the buckling temperatures with loading pattern 1 are quite low and displacements grow fast immediately after the temperature rises. This can however also be a consequence of coarse element mesh in the liner, which cannot deal with small displacement variations near the top weld, thus the liner may buckle prematurely. The remeshing of the calculation model revealed that the buckling temperature rose to just over 30°C when no initial perturbation was introduced. The buckling shape was also different compared to the model with coarser mesh. The comparison can be seen in Figure 26. The simulations with initial perturbations did not show such behavior when finer mesh was tested even though the development of the buckling shapes were slightly faster in some cases. Their buckling temperatures or shapes were not affected by the mesh refinement, so the analytical solution predicted surprisingly well the buckling temperature for them.

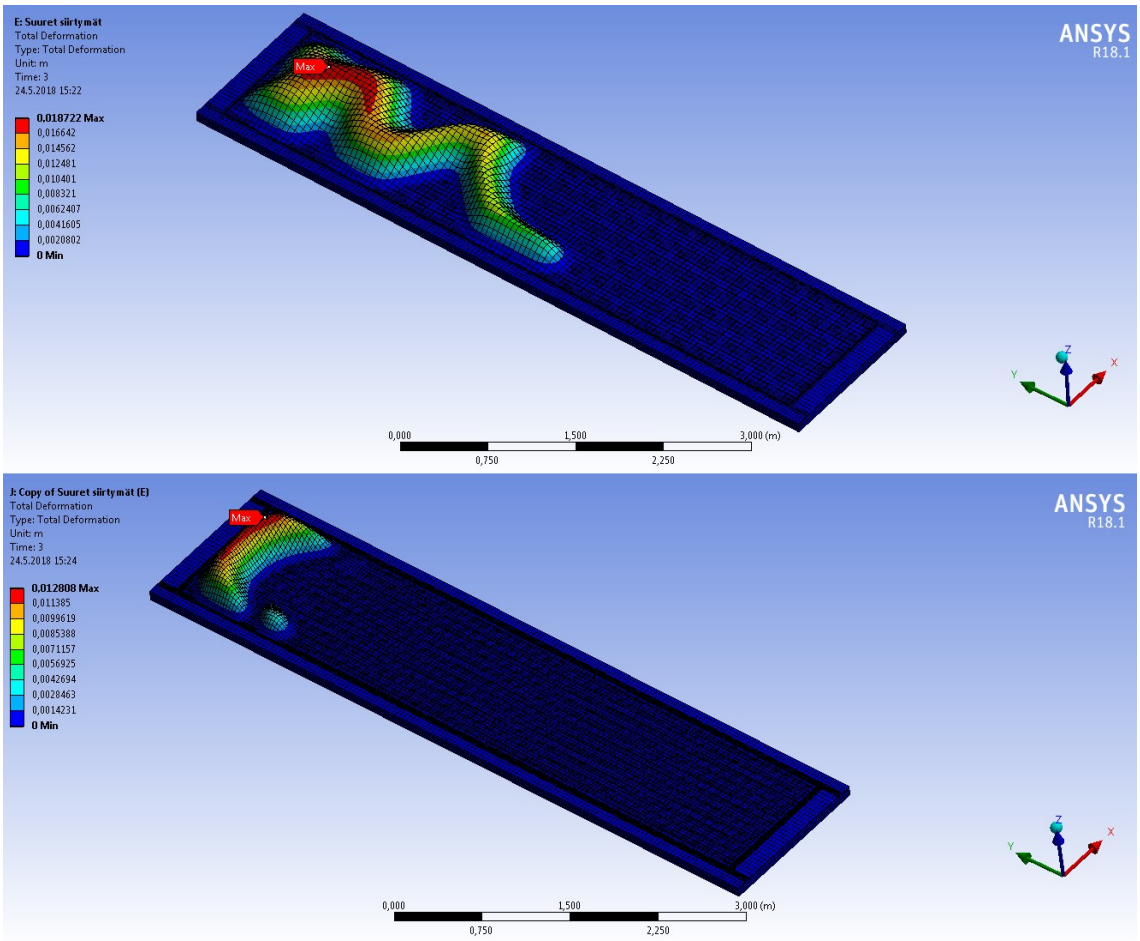

Figure 26. *Total deformation of coarse (upper) and fine mesh models at 45°C. The both models are calculation models CM1 with loading pattern 1. There is no initial perturbation applied. The displacements are not scaled by the same factor.*

The element mesh refinement was tested with pool floor plates as well but no variation in buckling shape or temperature was found. However, when the top weld was modified from imperfect fillet weld to resemble the actual groove weld in the bottom assembly, the liner plate did not buckle as early as with the initial model's 51.5°C. As a matter of fact, it did not buckle even at the temperature of 100°C. This happened with both mesh densities when tested. It should be noted that in reality, the welds are not fully symmetrical and may include various imperfections, so the buckling of the floor plates may be possible even with temperatures below 68°C.

5.4 Temperature varying yield strength

The analytical model predicted some plastic deformation in the floor liner plates when yield strength was lowered due to temperature effects, but it doesn't take account buckling behavior which may relieve the principal stresses in the liner. Also, the buckling of the

plate induces stress peaks which may cause plastic deformation areas in the liner or in the weld beads. To find out if the weld seam is still the most critical part of the assembly even with decreased liner yield strength, another numerical analysis was run with temperature varying material.

The liner buckled and as a result reached its plastic region at around 52°C, the strains in the welds were still by far higher compared to the liner. Therefore, it can be assumed that the most critical parts of the analyzed assembly are still the weld seams. When one of the floor plate's welds is an imperfect fillet weld, the liner plate buckles even with the most intense applicable water pressure when it is heated enough. This restricts the growth of the principal stresses acting on it.

This however, is not the case when 6 mm groove is added to the concrete block i.e. calculation model CM2 is employed. As the water pressure holds the liner plate in a concave form, it does not buckle before 68°C as can be seen in Figure 22. When the plate is not allowed to buckle, it will start to form plastic deformation areas due to the increase in principal stresses. The linear interpolation of the yield strength in chapter 5.2 predicted the yield temperature to be 61°C but did not include the deformation due to 6 mm cavity and water pressure. To find the solution for this case, calculation model CM2 with loading pattern 2 was solved with temperature varying material model and without weld imperfections. The only material property which was varied as a function of temperature was the yield strength. The elastic modulus could have been another relevant property to be varied but its effect is so small that it is negligible. Besides, the value of elastic modulus at 20°C produces conservative results since it reduces when temperature is increased.

At 45°C the maximum equivalent total strain peak in the weld bead was found to be approximately 0.3 % but the critical component seemed to be the liner plate when elemental mean strains were checked. Plastic deformation started to form in the liner already when the water pressure was applied. Figure 27 shows the plastic strain development in the metal parts and in Figure 28 the plastic regions of the liner, when water pressure is acting but temperature is not yet risen, are presented.

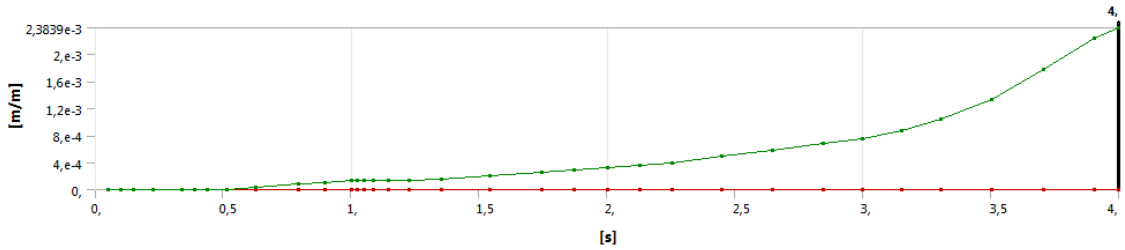

Figure 27. *Equivalent plastic strain development of calculation model CM2, loading pattern 2 with temperature varying material model. The liner starts to form plastic regions even before temperature is risen because water pressure pushes it against the 6 mm cavity.*

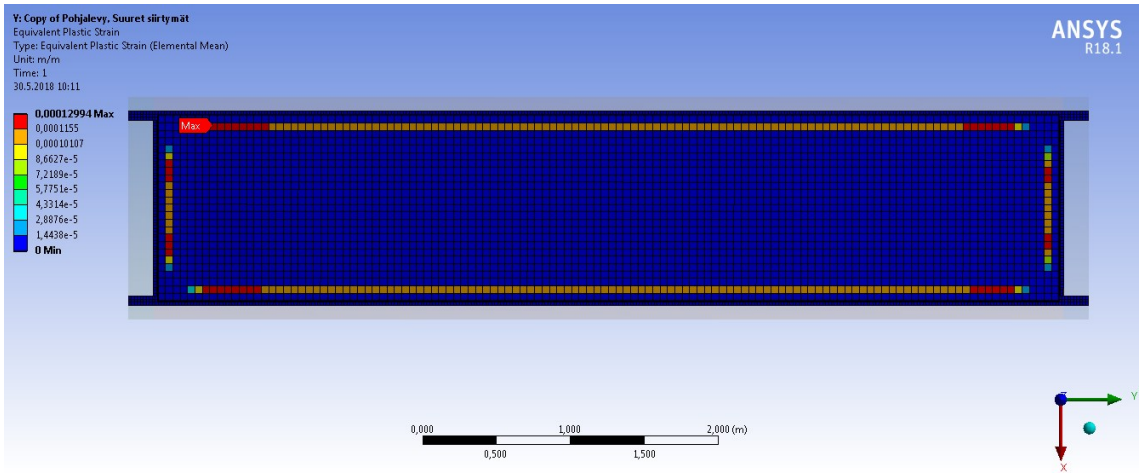

Figure 28. *Elemental mean plastic strain of the calculation model CM2, loading pattern 2 with temperature varying material model at 15°C. The water pressure has been applied entirely.*

Even though the simulated liner started to yield even before it was heated up, it is not probable in the real-life situation since the manufacturing error in the concrete block is quite exaggerated. As can be seen in Figure 4, the whole flange of the L-profile stud should be above the concrete surface for this initial case to exist. And as is evident from Figure 28, the plastic regions develop near the 6 mm step created by the L-profiles. Nevertheless, the 6 mm manufacturing tolerance is definitely plausible when the concrete surface does not include any large steps. Therefore, when the weld durability is not considered, the most critical initial condition for the liner plate is high water pressure combined with a cavity in the concrete slab. In that case the buckling of the plate does not occur and relieve the membrane stresses which eventually cause plastic deformations.

The decreased liner yield strength did not affect the outcome of the pool bottom assembly for the calculation model CM1; therefore the wall liner plate should not behave any differently since it buckles already at lower temperatures. Still an analysis with temperature varying yield strength was run to verify that assumption. In the analysis results the liner

plate's equivalent plastic strains, which concentrated into the buckling shape's most deflected segments near the welds, were slightly higher with reduced yield strength. The increase however was so insignificant that it did not have any influence on the displacement shape or on the result outcome whatsoever. As supposed, the weld strains were dominating in this case as well.

5.5 Results at 68°C

The maximum equivalent strain for each initial condition is listed in Table 16 and their triaxial corrected counterparts in Table 17. The largest strains can be seen to be induced by loading pattern 2 with the calculation model CM1. As mentioned in the end of chapter 5.3, the liner plate did not buckle with loading pattern 2 when the model's top weld was modified to have no imperfections. Even though the strains were relatively high according to the initial results at 68°C, they can be considered to not be perfectly valid due to premature buckling caused by unrealistic top weld. However, if the temperature is to be raised to around 50 degrees or above, it should be kept in mind that major imperfections in the pool bottom welds may cause buckling, large strain peaks and eventually failure of the welds. The results of the calculation model CM2 show how much smaller the strain values are when the liner plate does not buckle.

If the weld imperfections are not considered, the loading pattern 1 i.e. the wall plate seemed to generate the highest strains at 68°C as well, so it is deemed to be the most critical loading pattern. It can also be noted that the variations in triaxial corrected strains between the wall plate analyses are not very extensive, implying that small initial perturbations do not affect the liner plate's ultimate capacity by much even though the coarse mesh strains for initial perturbation 1 are somewhat larger compared to the other cases. To investigate if the initial perturbation 1 shows dissimilarity to the other results even with finer mesh, the simulation was run again with remeshed model. The buckling shape was found to be emerge earlier with increased number of elements which leads to a release of stresses and strains. No critical differences were found anymore with finer mesh for the case with initial perturbation 1.

The remeshed simulation of the wall plate without initial perturbations showed opposite results. As mentioned earlier, the buckling shape was not anymore similar to the coarse mesh model and it caused high deflection gradients in the liner plate. This in turn did not increase the equivalent strain maximum at 68°C but made the stress state highly more favorable to induce failure. The maximum triaxial corrected strain value was found to be 15.637 % for the remeshed model without initial perturbation implying that it is the most critical initial condition. However, it should be kept in mind that this buckling shape may not exist in any of the liner plates and the result analysis based on it is over conservative. Still it cannot be excluded so it has to be taken into account in the determination of temperature durability of the system.

Table 16. *Total equivalent strain maximums at 68°C of initial coarse meshed model. Results are expressed in percentage form.*

Calculation model CM1	**Loading pattern 1**	**Loading pattern 2**
No initial perturbation	2.74	5.78
1	2.06	-
2	2.75	-
3	3.35	4.35
4	-	-
Calculation model CM2		
No initial perturbation	2.73	0.66
5	3.23	-

Table 17. *Triaxial factor corrected strain maximums at 68°C of initial coarse meshed model. Results are expressed in percentage form.*

Calculation model CM1	**Loading pattern 1**	**Loading pattern 2**
No initial perturbation	3.43	4.19
1	4.94	-
2	2.75	-
3	3.35	4.35
4	-	-
Calculation model CM2		
No initial perturbation	2.73	0.66
5	3.23	-

As was the case with lower temperatures, the strains in the liner plate were not even close to the strains in the weld seams as can be seen in Table 18. It can be concluded that the

liner plate is not the first component to fail even though it may reach its yield strength in some cases.

Table 18. *Total equivalent liner plate strain maximums at 68°C of initial coarse meshed model. Results are expressed in percentage form.*

Calculation model CM1	**Loading pattern 1**	**Loading pattern 2**
No initial perturbation	0.52	0.49
1	0.43	-
2	0.40	-
3	0.49	0.47
4	-	-
Calculation model CM2		
No initial perturbation	0.40	0.56
5	0.33	-

5.6 Fatigue

The coolant temperature in the fuel pool stays normally at 30°C so the strain amplitude used in fatigue calculations should be the maximum equivalent strain difference between maintenance temperature and operating temperature. However, the strains at 30°C seems to be insignificant compared to the strain magnitude at the maintenance temperature allowing straight-forwardly the maximum strain values to be used. When different fatigue parameters from Table 4 and Table 5 are substituted into equation (***22***) and triaxial corrected strains are used, the expected maximum life values for the analyzed geometry are acquired.

As mentioned, the normal annual maintenance temperature reaches only 42°C but the major maintenance shutdown or malfunction in the cooling system increases the coolant temperature even more. Table 19 shows cumulative damage values for annual maintenances and different peak temperatures which are assumed to take place only once during the life cycle of Olkiluoto 1&2 power plants. The annual maintenance temperature has been roughly 42°C last 40 cycles as reported by the measurement data but if it can be raised in the future, power increase of the plants can be executed without modifications

to the liner assemblies. Also, the maintenance and fuel replacement procedures get more efficient if temperature limit is not very strict. Therefore, higher annual maintenance temperatures are also considered. The values in Table 19 are based on the damaging effect of the temperature increases and they are modeled using Palmgren-Miner rule, which was introduced earlier in chapter 3.6. The nominal strains used in the fatigue calculations are from the most critical initial condition found in the numerical simulations: from the remeshed calculation model CM1 with loading pattern 1 and without initial perturbations.

Table 19. *Damage parameter values for different cyclic conditions for calculation model CM1, loading pattern 1 without initial perturbations. Total number of cycles is 80. The first 40 strain amplitudes are based on the results at 42°C. The values are in expressed in percentage form.*

Proposed annual maintenance temperature in the future	Peak temperature: No peak	55°C	60°C	68°C
42°C	32.9	35.3	36.3	39.5
45°C	47.2	49.7	50.7	53.9
50°C	77.8	80.3	81.3	84.5
55°C	113.5	116.0	117.0	120.1

It is evident that a single extreme coolant temperature value does not reduce the life of the liner assembly immensely. Between one 68°C peak and absence of the temperature peak, there is only a difference of 6.6 percentage points. As the Palmgren-Miner rule is linear summation, the effect of multiple temperature peaks is easily found by multiplying the effect of a single peak. For example, with 42°C normal annual maintenance temperature and with 5 separate 68°C peaks, the damage parameter can be calculated to be roughly 65.9 %. The change in normal annual maintenance temperature makes more significant impact to the damage parameter. Only a small temperature increase results in a relatively large reduction in the life of the geometry because the temperature – strain relation is slightly nonlinear and the number of annual maintenance cycles is quite high. This can be seen in Figure 29, where a quadratic line is fitted into the fatigue result points of the situation with one 68°C temperature peak. The fitted equation reaches 100 % at approximate temperature of 52.3°C.

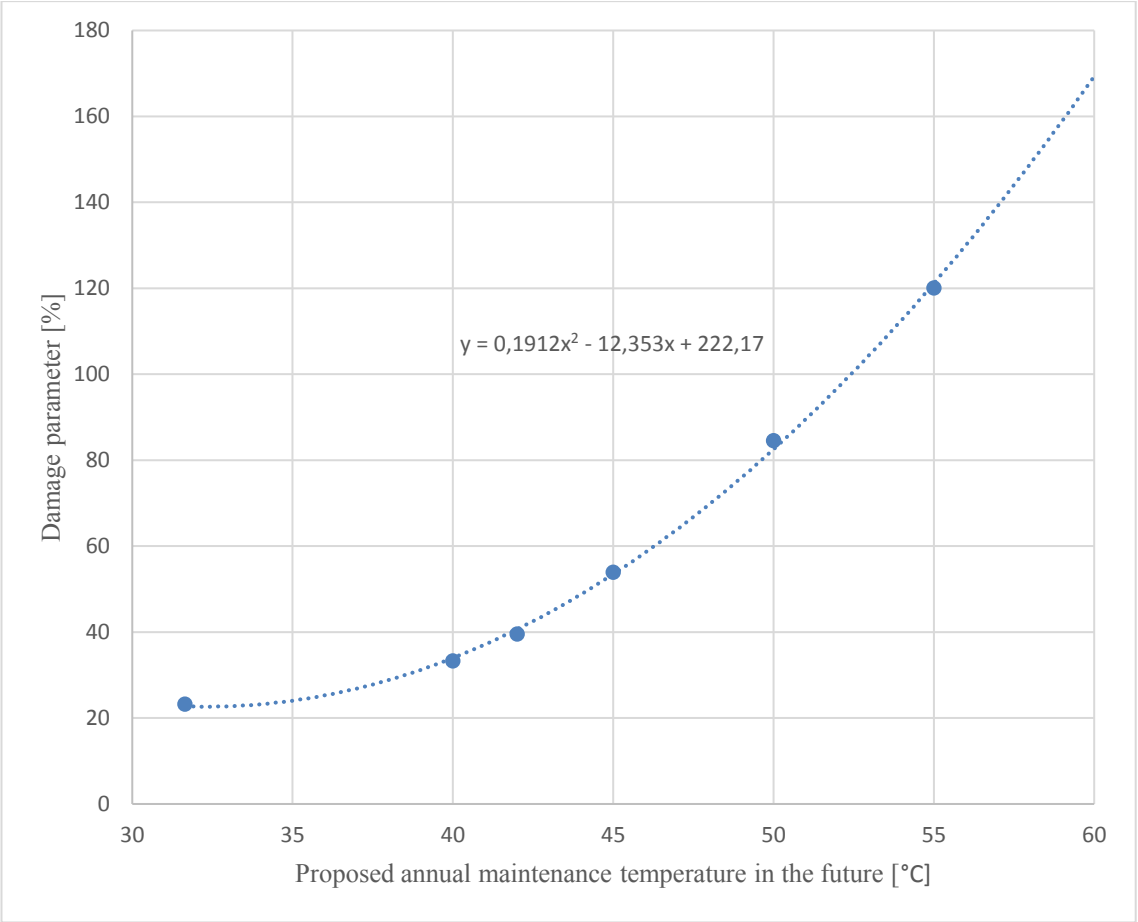

Figure 29. *Damage parameter with respect to annual maintenance temperature for the next 40 years. In this graph a single 68°C temperature peak is taken into account.*

As discussed in the result section of monotonic loadings, the maximum nominal strain of the numerical model was found in the weld beads. However, the fatigue properties for weld material was assumed to be identical to stainless-steel. This may produce inaccuracy to the fatigue results due to imperfect and heterogenous nature of welds, thus safety margin is recommended. Additionally, some error is generated by the fact that it is assumed that normal annual maintenance temperature induced strain maximum is at the same position as the strain peak caused by the abnormally high temperature, even though they truly are not. This however does not have a large impact since a single peak temperature was found to have only a small effect to the overall life. It also makes the solution to be more conservative, so the generated inaccuracy is on the safe side.

6. CONCLUSION

A nuclear fuel pool steel liner integrity at normal and abnormal temperatures was analyzed using analytical and numerical methods. The numerical simulations were done with multiple initial conditions and perturbations and element mesh density was varied for sensitivity test purposes. Buckling of the liner plates was covered in both, analytic and numerical calculations using plate theory and nonlinear FEM-models respectively. The failure criterion was chosen to be a strain-based limit due to plastic behavior at higher temperatures. Also, fatigue durability of the liner was approximated with low-cycle fatigue theory. Total lifetime of the nuclear power plant was assumed to be 80 years with 40 years of operation still ahead.

The added initial perturbations in the FEM-model did not seem to have substantial impact on the result outcome since the most critical initial condition was found to be the one without any perturbations. The perturbations incited the liner plate's buckling shape to develop easier thus stress growth was inhibited. When sensitivity study was done, it was found that the element mesh accuracy affected the results. The buckling temperature, buckling shape and maximum strain values varied to some extent with mesh refinement so it can be reasoned that the initial mesh density was too coarse for the calculations. Despite that, the results with finer mesh appeared to be quite consistent and trustworthy.

The largest factor in the result outcome was the loading pattern. Two different loading patterns were analyzed and they were based on the positions of the liner plates in the fuel pool. After some verifying calculations, wall plates were found to fail before floor plates. However, floor plate simulation showed high strain maximums when one of the welds was modeled as an imperfect fillet weld instead of groove weld. High strain maximus were due to high water pressure and buckling which was induced by the imperfect weld roughly at 51°C.

All in all, liner plate near the coolant water surface without any initial perturbation was found to be the most critical section of the fuel pool according to the chosen failure criterion. More specifically, the areas of the side welds near the buckling shape started to fail first. The highest temperature considered in this study was 68°C, which did not lead to the failure of the liner per se but increased the probability of fatigue failure.

Even though one single temperature peak did not break the liner assembly, temperature limit increase during annual maintenance procedures was found to have significant impact to the fatigue life of the liner assemblies. The maximum temperature limit for future maintenances according to the fatigue calculation outcome was roughly 52°C. This result however does not include any safety factors. Due to inaccurate material properties and

stochastic character of welds some error is apparent, but it is tried to counteract by applying conservative assumptions whenever feasible and appropriate. Based on the fatigue results, the annual maintenance temperature of 42°C which is currently practiced, was found to utilize approximately 33 % of the liner assembly's structural capacity.

BIBLIOGRAPHY

[1] Nuclear Power in the World Today, World Nuclear Association, web page. Available (accessed 10.07.2018): http://www.world-nuclear.org/information-library/current-and-future-generation/nuclear-power-in-the-world-today.aspx.

[2] Ydinvoimalaitosyksiköt Olkiluoto 1 ja Olkiluoto 2, Teollisuuden Voima, 2007.

[3] IAEA Nuclear Energy Series Publications, International Atomic Energy Agency, Vienna, 2011, 136 p.

[4] E. Johansson, The effect of an allowable crack width on concrete structures of pools in nuclear facilities, Aalto University, Department of Civil and Structural Engineering, 2013, 79 p.

[5] L. Andersson, TVO, Temperature Analysis, OL1/OL2 - Investigation of crack widths due to temperature increase in the fuel pools, Scanscot Technology AB, Lund, 2017, 64 p.

[6] Regulatory Guides on nuclear safety and security (YVL), STUK - Radiation and Nuclear Safety Authority, web page. Available (accessed 10.07.2018): http://www.stuk.fi/web/en/regulations/stuk-s-regulatory-guides/regulatory-guides-on-nuclear-safety-yvl-.

[7] KTA 2502, Mechanical Design of Fuel Assembly Storage Pools in Nuclear Power Plants with Light Water Reactors, KTA-Geschaeftsstelle, Salzgitter, 2011.

[8] EN 1993-1-4, Eurocode 3: Design of steel structures - Part 1-4: General rules - Supplementary rules for stainless steels, European committee for standardization, Brussels, 2006.

[9] EN 1993-1-5 Eurocode 3: Design of steel structures - Part 1-5: Plated structural elements, European committee for standardization, Brussels, 2006.

[10] 2017 ASME Boiler & Pressure Vessel Code III Division 2, Rules for Construction of Nuclear Facility Components - Code for Concrete Containments, The American Society of Mechanical Engineers, New York, 2017.

[11] TVO Olkiluoto II, Reaktorinsuojarakennus, Altaat peltipäällyste, yksityiskohtia, 201-22-121/2, Asea-Atom, 1976.

[12] SFS-EN 10088-1, Stainless steels. Part 1: List of stainless steels, Finnish Standards Association, Helsinki, 2014.

[13] SFS-EN 10088-2, Stainless steels. Part 2: Technical delivery conditions for sheet/plate and strip of corrosion resisting steels for general purposes, Finnish Standards Association, Helsinki, 2014.

[14] Technical card - 1.4301, Lucefin group, 2012.

[15] Welding filler metal handbook, ESAB, 2016.

[16] T. Kukkola, Chief engineer, Civil Engineering, Teollisuuden Voima, Interview date (28.02.2018).

[17] ANSYS Help Viewer 18.1.0, SAS IP, Inc., 2017.

[18] S. Timoshenko, J. Gere, Theory of Elastic Stability, Second ed. McGraw-Hill, New York, 1961, 541 p.

[19] E. Davis, F. Connelly, Stress Distribution and Plastic Deformation in Rotating Cylinders of Strain Hardening Material, Journal of Applied Mechanics, Vol. 81, 1959, pp. 25-30.

[20] S. Manson, G. Halford, Discussion of paper by J.J. Blass and S. Y. Zamrik, entitled "Multiaxial Low-Cycle Fatigue of Type 304 Stainless Steel", Journal of Engineering Materials and Technology, Vol. 99, 1977, pp. 283-286.

[21] L. Coffin, A Study of the Effects of Cyclic Thermal Stresses on a Ductile Metal, Knolls Atomic Power Laboratory, New York, 1953, 129 p. Available: http://www.osti.gov/scitech/biblio/4363016.

[22] S. Manson, Behavior of materials under conditions of thermal stress, National Advisory Committee for Aeronautics, Washington, D.C, 1953, 105 p.

[23] O. Basquin, The Exponential Law of Endurance Tests, American Society for Testing and Materials Proceedings, Vol. 10, 1910, pp. 625-630.

[24] A. Bäumel, T. Seeger, Materials data for cyclic loading. Supplement 1, Elsevier Science Publishers, Amsterdam, 1990.

[25] OL2 243-altaiden lämpötiloja vuosihuollon aikaan, Teollisuuden Voima, internal memorandum.

[26] M. Miner, Cumulative damage in fatigue, Journal of Applied Mechanics, Vol. 67, 1945, pp. 159-164.

[27] R. von Mises, Mechanik der festen Körper im plastisch deformablen Zustand, Nachrichten von der Gesellschaft der Wissenschaften zu Göttingen, Mathematisch-Physikalische Klasse, 1913, pp. 582-592.